3GPP TR 38.901 V16.1.0 (2019-12)

Technical Report

**3rd Generation Partnership Project;
Technical Specification Group Radio Access Network;
Study on channel model for frequencies from 0.5 to 100 GHz
(Release 16)**

Keywords
New Radio

3GPP

Postal address

3GPP support office address
650 Route des Lucioles - Sophia Antipolis Valbonne - FRANCE Tel.: +33 4 92 94 42 00 Fax: +33 4 93 65 47 16

Internet
http://www.3gpp.org

3GPP

Contents

Foreword

This Technical Report has been produced by the 3rd Generation Partnership Project (3GPP).

The contents of the present document are subject to continuing work within the TSG and may change following formal TSG approval. Should the TSG modify the contents of the present document, it will be re-released by the TSG with an identifying change of release date and an increase in version number as follows:

Version x.y.z

where:

x the first digit:

   1 presented to TSG for information;

   2 presented to TSG for approval;

   3 or greater indicates TSG approved document under change control.

y the second digit is incremented for all changes of substance, i.e. technical enhancements, corrections, updates, etc.

z the third digit is incremented when editorial only changes have been incorporated in the document.

1   Scope

The present document captures the findings of the study item, "Study on channel model for frequency spectrum above 6 GHz" [2] and from further findings of the study item, "Study on New Radio Access Technology [22]" and the study item "Study on Channel Modeling for Indoor Industrial Scenarios [23]". The channel models in the present document address the frequency range 0.5-100 GHz. The purpose of this TR is to help TSG RAN WG1 to properly model and evaluate the performance of physical layer techniques using the appropriate channel model(s). Therefore, the TR will be kept up-to-date via CRs in the future.

This document relates to the 3GPP evaluation methodology and covers the modelling of the physical layer of both Mobile Equipment and Access Network of 3GPP systems.

This document is intended to capture the channel model(s) for frequencies from 0.5GHz up to 100GHz.

2   References

The following documents contain provisions which, through reference in this text, constitute provisions of the present document.

- References are either specific (identified by date of publication, edition number, version number, etc.) or non-specific.

- For a specific reference, subsequent revisions do not apply.

- For a non-specific reference, the latest version applies. In the case of a reference to a 3GPP document (including a GSM document), a non-specific reference implicitly refers to the latest version of that document *in the same Release as the present document*.

[1]   3GPP TR 21.905: "Vocabulary for 3GPP Specifications".

[2]   3GPP TD RP-151606: "Study on channel model for frequency spectrum above 6 GHz".

[3]   3GPP TR 36.873 (V12.2.0): "Study on 3D channel model for LTE".

[4]   3GPP RP-151847: "Report of RAN email discussion about >6GHz channel modelling", Samsung.

[5]   3GPP TD R1-163408: "Additional Considerations on Building Penetration Loss Modelling for 5G System Performance Evaluation", Straight Path Communications.

[6]   ICT-317669-METIS/D1.4: "METIS channel model, METIS 2020, Feb, 2015".

[7]   Glassner, A S: "An introduction to ray tracing. Elsevier, 1989".

[8]   McKown, J. W., Hamilton, R. L.: "Ray tracing as a design tool for radio networks, Network, IEEE, 1991(6): 27-30".

[9]   Kurner, T., Cichon, D. J., Wiesbeck, W.: "Concepts and results for 3D digital terrain-based wave propagation models: An overview", IEEE J.Select. Areas Commun., vol. 11, pp. 1002–1012, 1993.

[10]   Born, M., Wolf, E.: "Principles of optics: electromagnetic theory of propagation, interference and diffraction of light", CUP Archive, 2000.

[11]   Friis, H.: "A note on a simple transmission formula", proc. IRE, vol. 34, no. 5, pp. 254–256, 1946.

[12]   Kouyoumjian, R.G., Pathak, P.H.: "A uniform geometrical theory of diffraction for an edge in a perfectly conducting surface" Proc. IEEE, vol. 62, pp. 1448–1461, Nov. 1974.

[13]   Pathak, P.H., Burnside, W., Marhefka, R.: "A Uniform GTD Analysis of the Diffraction of Electromagnetic Waves by a Smooth Convex Surface", IEEE Transactions on Antennas and Propagation, vol. 28, no. 5, pp. 631–642, 1980.

[14]   IST-WINNER II Deliverable 1.1.2 v.1.2, "WINNER II Channel Models", IST-WINNER2, Tech. Rep., 2007 (http://www.ist-winner.org/deliverables.html).

[15]   3GPP TR36.101: "User Equipment (UE) radio transmission and reception".

[16]   3GPP TR36.104: "Base Station (BS) radio transmission and reception".

[17]   Asplund, H., Medbo, J., Göransson, B., Karlsson, J., Sköld, J.: "A simplified approach to applying the 3GPP spatial channel model", in Proc. of PIMRC 2006.

[18]   ITU-R Rec. P.1816: "The prediction of the time and the spatial profile for broadband land mobile services using UHF and SHF bands".

[19]   ITU-R Rec. P.2040-1: "Effects of building materials and structures on radiowave propagation above about 100 MHz", International Telecommunication Union Radiocommunication Sector ITU-R, 07/2015.

[20]   ITU-R Rec. P.527-3: "Electrical characteristics of the surface of the earth", International Telecommunication Union Radiocommunication Sector ITU-R, 03/1992.

[21]   Jordan, E.C., Balmain, K.G.: "Electromagnetic Waves and Radiating Systems", Prentice-Hall Inc., 1968.

[22]   3GPP TD RP-162469: "Study on New Radio (NR) Access Technology".

[23]   3GPP TD RP-182138: "SID on Channel Modeling for Indoor Industrial Scenarios".

3   Definitions, symbols and abbreviations

3.1   Definitions

For the purposes of the present document, the terms and definitions given in TR 21.905 [1] apply.

3.2   Symbols

For the purposes of the present document, the following symbols apply:

A	antenna radiation power pattern
A_{max}	maximum attenuation
d_{2D}	2D distance between Tx and Rx
d_{3D}	3D distance between Tx and Rx
d_H	antenna element spacing in horizontal direction
d_V	antenna element spacing in vertical direction
f	frequency
f_c	center frequency / carrier frequency
$F_{\mathrm{rx,u},\theta}$	Receive antenna element u field pattern in the direction of the spherical basis vector $\hat{\theta}$
$F_{\mathrm{rx,u},\phi}$	Receive antenna element u field pattern in the direction of the spherical basis vector $\hat{\phi}$
$F_{\mathrm{tx,s},\theta}$	Transmit antenna element s field pattern in the direction of the spherical basis vector $\hat{\theta}$
$F_{\mathrm{rx,s},\phi}$	Transmit antenna element s field pattern in the direction of the spherical basis vector $\hat{\phi}$
h_{BS}	antenna height for BS
h_{UT}	antenna height for UT
$\hat{r}_{rx,n,m}$	spherical unit vector of cluster n, ray m, for receiver
$\hat{r}_{tx,n,m}$	spherical unit vector of cluster n, ray m, for transmitter
α	bearing angle

β	downtilt angle
γ	slant angle
λ	wavelength
κ	cross-polarization power ratio in linear scale
μ_{lgASA}	mean value of 10-base logarithm of azimuth angle spread of arrival
μ_{lgASD}	mean value of 10-base logarithm of azimuth angle spread of departure
μ_{lgDS}	mean value of 10-base logarithm of delay spread
μ_{lgZSA}	mean value of 10-base logarithm of zenith angle spread of arrival
μ_{lgZSD}	mean value of 10-base logarithm of zenith angle spread of departure
$\Pr_{LOS}$	LOS probability
SLA_V	side-lobe attenuation in vertical direction
σ_{lgASA}	standard deviation of 10-base logarithm of azimuth angle spread of arrival
σ_{lgASD}	standard deviation of 10-base logarithm of azimuth angle spread of departure
σ_{lgDS}	standard deviation value of 10-base logarithm of delay spread
σ_{lgZSA}	standard deviation of 10-base logarithm of zenith angle spread of arrival
σ_{lgZSD}	standard deviation of 10-base logarithm of zenith angle spread of departure
σ_{SF}	standard deviation of SF
ϕ	azimuth angle
θ	zenith angle
$\hat{\phi}$	spherical basis vector (unit vector) for GCS
$\hat{\phi}'$	spherical basis vector (unit vector) for LCS
ϕ_{3dB}	horizontal 3 dB beamwidth of an antenna
$\hat{\theta}$	spherical basis vector (unit vector), orthogonal to $\hat{\phi}$, for GCS
$\hat{\theta}'$	spherical basis vector (unit vector), orthogonal to $\hat{\phi}'$, for LCS
θ_{etilt}	electrical steering angle in vertical direction
θ_{3dB}	vertical 3 dB beamwidth of an antenna
ψ	Angular displacement between two pairs of unit vectors

3.3 Abbreviations

For the purposes of the present document, the abbreviations given in TR 21.905 [1] and the following apply. An abbreviation defined in the present document takes precedence over the definition of the same abbreviation, if any, in TR 21.905 [1].

2D	two-dimensional
3D	three-dimensional
AOA	Azimuth angle Of Arrival
AOD	Azimuth angle Of Departure
AS	Angular Spread
ASA	Azimuth angle Spread of Arrival
ASD	Azimuth angle Spread of Departure
BF	Beamforming
BS	Base Station
BP	Breakpoint
BW	Beamwidth
CDF	Cumulative Distribution Function
CDL	Clustered Delay Line
CRS	Common Reference Signal
D2D	Device-to-Device
DFT	Discrete Fourier Transform
DS	Delay Spread
GCS	Global Coordinate System

IID	Independent and identically distributed
InF	Indoor Factory
InF-SL	Indoor Factory with Sparse clutter and Low base station height (both Tx and Rx are below the average height of the clutter)
InF-DL	Indoor Factory with Dense clutter and Low base station height (both Tx and Rx are below the average height of the clutter)
InF-SH	Indoor Factory with Sparse clutter and High base station height (Tx or Rx elevated above the clutter)
InF-DH	Indoor Factory with Dense clutter and High base station height (Tx or Rx elevated above the clutter)
InF-HH	Indoor Factory with High Tx and High Rx (both elevated above the clutter)
InH	Indoor Hotspot
IRR	Infrared Reflecting
ISD	Intersite Distance
K	Ricean K factor
LCS	Local Coordinate System
LOS	Line Of Sight
MIMO	Multiple-Input-Multiple-Output
MPC	Multipath Component
NLOS	Non-LOS
O2I	Outdoor-to-Indoor
O2O	Outdoor-to-Outdoor
OFDM	Orthogonal Frequency-Division Multiplexing
PAS	Power angular spectrum
PL	Path Loss
PRB	Physical Resource Block
RCS	Radar cross-section
RMa	Rural Macro
RMS	Root Mean Square
RSRP	Reference Signal Received Power
Rx	Receiver
SCM	Spatial Channel Model
SINR	Signal-to-Interference-plus-Noise Ratio
SIR	Signal-to-Interference Ratio
SSCM	Statistical Spatial Channel Model
SF	Shadow Fading
SLA	Sidelobe Attenuation
TDL	Tapped Delay Line
TOA	Time Of Arrival
TRP	Transmission Reception Point
Tx	Transmitter
UMa	Urban Macro
UMi	Urban Micro
UT	User Terminal
UTD	Uniform Theory of Diffraction
V2V	Vehicle-to-Vehicle
XPR	Cross-Polarization Ratio
ZOA	Zenith angle Of Arrival
ZOD	Zenith angle Of Departure
ZSA	Zenith angle Spread of Arrival
ZSD	Zenith angle Spread of Departure

4   Introduction

At 3GPP TSG RAN #69 meeting the Study Item Description on "Study on channel model for frequency spectrum above 6 GHz" was approved [2]. This study item covers the identification of the status/expectation of existing information on high frequencies (e.g. spectrum allocation, scenarios of interest, measurements, etc), and the channel model(s) for frequencies up to 100 GHz. This technical report documents the channel model(s). The new channel model has to a large degree been aligned with earlier channel models for <6 GHz such as the 3D SCM model (3GPP TR

36.873) or IMT-Advanced (ITU-R M.2135). The new model supports comparisons across frequency bands over the range 0.5-100 GHz. The modelling methods defined in this technical report are generally applicable over the range 0.5-100 GHz, unless explicitly mentioned otherwise in this technical report for specific modelling method, involved parameters and/or scenario.

Subsequently, at the 3GPP TSG RAN #81 meeting the Study Item Description "Study on Channel Modeling for Indoor Industrial Scenarios" was approved [23]. The findings from this study item is also captured in the present technical report. The Industrial channel model was developed by considering new measurements and information in the literature. An overview list of all such contributions and sources is available in tdoc R1-1909706.

The channel model is applicable for link and system level simulations in the following conditions:

- For system level simulations, supported scenarios are urban microcell street canyon, urban macrocell, indoor office, rural macrocell, and indoor factory.

- Bandwidth is supported up to 10% of the center frequency but no larger than 2GHz.

- Mobility of either one end of the link or both ends of the link is supported

- For the stochastic model, spatial consistency is supported by correlation of LSPs and SSPs as well as LOS/NLOS state.

- Large array support is based on far field assumption and stationary channel over the size of the array.

5 General

6 Status/expectation of existing information on high frequencies

6.1 Channel modelling works outside of 3GPP

This clause summarizes the channel modelling work outside of 3GPP based on the input from companies.

Groups and projects with channel models:

- METIS (Mobile and wireless communications Enablers for the Twenty-twenty Information Society)

- MiWEBA (Millimetre-Wave Evolution for Backhaul and Access)

- ITU-R M

- COST2100

- IEEE 802.11

- NYU WIRELESS: interdisciplinary academic research center

- Fraunhofer HHI has developed the QuaDRiGa channel model, Matlab implementation is available at http://quadriga-channel-model.de

Groups and projects which intend to develop channel models:

- 5G mmWave Channel Model Alliance: NIST initiated, North America based

- mmMAGIC (Millimetre-Wave Based Mobile Radio Access Network for Fifth Generation Integrated Communications): Europe based

- IMT-2020 5G promotion association: China based

METIS Channel Models:
- Identified 5G requirements (e.g., wide frequency range, high bandwidth, massive MIMO, 3-D and accurate polarization modelling)

- Performed channel measurements at various bands between 2GHz and 60 GHz

- Provided different channel model methodologies (map-based model, stochastic model or hybrid model). For stochastic model, the proposed channel is focused on outdoor square, Indoor cafeteria and indoor shopping mall scenarios.

MiWEBA Channel Models:
- Addressed various challenges: Shadowing, spatial consistency, environment dynamics, spherical wave modelling, dual mobility Doppler model, ratio between diffuse and specular reflections, polarization

- Proposed Quasi-deterministic channel model

- Performed channel measurements at 60 GHz

- Focused on university campus, street canyon, hotel lobby, backhaul, and D2D scenarios.

ITU-R M Channel Models:
- Addressed the propagation loss and atmospheric loss on mmW

- Introduced enabling antenna array technology and semiconductor technology

- Proposed deployment scenarios, focused on dense urban environment for high data rate service: indoor shopping mall, indoor enterprise, in home, urban hotspot in a square/street, mobility in city.

COST2100 and COST IC1004 Channel Models:
- Geometry-based stochastic channel model that reproduce the stochastic properties of MIMO channels over time, frequency and space. It is a cluster-level model where the statistics of the large scale parameters are always guaranteed in each series of channel instances.

NYU WIRELESS Channel Models:
- Conducted many urban propagation measurements on 28/38/60/73 GHz bands for both outdoor and indoor channels, measurements are continuing.

- Proposed 3 areas for 5G mmWave channel modelling which are small modifications or extensions from 3GPP's current below 6GHz channel models

- 1) LOS/NLOS/blockage modelling (a squared exponential term); 2). Wideband power delay profiles (time clusters and spatial lobes for a simple extension to the existing 3GPP SSCM model); 3). Physics-based path loss model (using the existing 3GPP path loss equations, but simply replacing the "floating" optimization parameter with a deterministic 1 m "close-in" free space reference term in order to provide a standard and stable definition of "path loss exponent" across all different parties, scenarios, and frequencies).

802.11 ad/ay Channel Models:
- Conducted ray-tracing methodology on 60 GHz band indoor channels, including conference room, cubicle, living room scenarios

- Intra cluster parameters were proposed in terms of ray excess delay and ray power distribution

- Human blockage models were proposed in terms of blockage probability and blockage attenuation

5G mmWave Channel Model Alliance:
- Will provide a venue to promote fundamental research into measurement, analysis, identification of physical parameters, and statistical representations of mmWave propagation channels.

- Divided into six collaborative working groups that include a Steering Committee; Modelling Methodology Group; Measurement Methodology Group; and groups that focus on defining and parameterizing Indoor, Outdoor, and Emerging Usage Scenarios.

- Sponsored by Communications Technology Research Laboratory within the NIST.

mmMAGIC:
- Brings together major infrastructure vendors, major European operators, leading research institutes and universities, measurement equipment vendors and one SME.

- Will undertake extensive radio channel measurements in the 6-100 GHz range.

- Will develop and validate advanced channel models that will be used for rigorous validation and feasibility analysis of the proposed concepts and system, as well as for usage in regulatory and standards fora.

IMT-2020 5G promotion association
- Jointly established by three ministries of China based on the original IMT-Advanced promotion group

- Members including the main operators, vendors, universities and research institutes in China

- The major platform to promote 5G technology research in China and to facilitate international communication and cooperation

QuaDRiGa (Fraunhofer HHI)
- QuaDRiGa (QUAsi Deterministic RadIo channel GenerAtor) was developed at the Fraunhofer Heinrich Hertz Institute within the Wireless Communications and Networks Department to enable the modelling of MIMO radio channels for specific network configurations, such as indoor, satellite or heterogeneous configurations.

- Besides being a fully-fledged 3D geometry-based stochastic channel model (well aligned with TR36.873), QuaDRiGa contains a collection of features created in SCM(e) and WINNER channel models along with novel modelling approaches which provide features to enable quasi-deterministic multi-link tracking of users (receiver) movements in changing environments. QuaDRiGa supports Massive MIMO modelling enabled through a new multi-bounce scattering approach and spherical wave propagation. It will be continuously extended with features required by 5G and frequencies beyond 6 GHz. The QuaDRiGa model is supported by data from extensive channel measurement campaigns at 10 / 28 / 43 / 60 / 82 GHz performed by the same group.

6.2   Scenarios of interest

Brief description of the key scenarios of interest identified (see note):

(1) UMi (Street canyon, open area) with O2O and O2I: This is similar to 3D-UMi scenario, where the BSs are mounted below rooftop levels of surrounding buildings. UMi open area is intended to capture real-life scenarios such as a city or station square. The width of the typical open area is in the order of 50 to 100 m.

Example: [Tx height:10m, Rx height: 1.5-2.5 m, ISD: 200m]

(2) UMa with O2O and O2I: This is similar to 3D-UMa scenario, where the BSs are mounted above rooftop levels of surrounding buildings.

Example: [Tx height:25m, Rx height: 1.5-2.5 m, ISD: 500m]

(3) Indoor: This scenario is intended to capture various typical indoor deployment scenarios, including office environments, and shopping malls. The typical office environment is comprised of open cubicle areas, walled offices, open areas, corridors etc. The BSs are mounted at a height of 2-3 m either on the ceilings or walls. The shopping malls are often 1-5 stories high and may include an open area (or "atrium") shared by several floors. The BSs are mounted at a height of approximately 3 m on the walls or ceilings of the corridors and shops.

Example: [Tx height: 2-3m, Rx height: 1.5m, area: 500 square meters]

(4) Backhaul, including outdoor above roof top backhaul in urban area and street canyon scenario where small cell BSs are placed at lamp posts.

(5) D2D/V2V. Device-to-device access in open area, street canyon, and indoor scenarios. V2V is a special case where the devices are mobile.

(6) Other scenarios such as Stadium (open-roof) and Gym (close-roof).

(7) Indoor industrial scenarios

Note: The scenarios of interest are based on the plenary email discussion and different from the supported scenarios in clause 7. The indoor industrial scenarios were identified at a later stage in the 3GPP TSG RAN #81 meeting.

6.3 Channel measurement capabilities

The measurement capability as reported by each company is summarized in the following table.

Table 6.3-1: Channel measurement capabilities

	6 - 20 GHz	20 - 30 GHz	30 - 60 GHz	>60 GHz
Urban macro	CMCC Nokia/Aalborg	Nokia/Aalborg	NYU	
Urban micro	Aalto University CMCC Ericsson Intel/Fraunhofer HHI Nokia/Aalborg NTT DOCOMO Orange	AT&T Aalto University CMCC Huawei Intel/Fraunhofer HHI Nokia/Aalborg NTT DOCOMO NYU Qualcomm Samsung CATT KT ETRI ITRI/CCU ZTE	AT&T Huawei Intel/Fraunhofer HHI NTT DOCOMO Qualcomm CATT ETRI ITRI/CCU ZTE	AT&T Aalto University Huawei Intel/Fraunhofer HHI NYU
Indoor	Aalto University CMCC Ericsson Huawei Intel/Fraunhofer HHI Nokia/Aalborg NTT DOCOMO Orange	AT&T Alcatel-Lucent Aalto University BUPT CMCC Huawei Intel/Fraunhofer HHI Nokia/Aalborg NTT DOCOMO NYU Qualcomm Samsung CATT KT ETRI ITRI/CCU ZTE	AT&T Ericsson Huawei Intel/Fraunhofer HHI NTT DOCOMO NYU Qualcomm CATT ETRI ITRI/CCU ZTE	AT&T Aalto University Huawei Intel/Fraunhofer HHI NYU
O2I	Ericsson Huawei Intel/Fraunhofer HHI Nokia/Aalborg NTT DOCOMO Orange	AT&T Alcatel-Lucent Ericsson Huawei Intel/Fraunhofer HHI NTT DOCOMO NYU Samsung KT	AT&T Ericsson Huawei Intel/Fraunhofer HHI NTT DOCOMO	AT&T Huawei Intel/Fraunhofer HHI

6.4 Modelling objectives

The requirements for channel modelling are as follows.

- Channel model SI should take into account the outcome of RAN-level discussion in the '5G' requirement study item

- Complexity in terms of Description, Generating channel coefficients, development complexity and Simulation time should be considered.

- Support frequency range up to 100 GHz.

  - The critical path of the SI is 6 – 100 GHz

  - Take care of mmW propagation aspects such as blocking and atmosphere attenuation.

- The model should be consistent in space, time and frequency

- Support large channel bandwidths (up to 10% of carrier frequency)

- Aim for the channel model to cover a range of coupling loss considering current typical cell sizes, e.g. up to km-range macro cells. Note: This is to enable investigation of the relevance of the 5G system using higher frequency bands to existing deployments.

- Accommodate UT mobility

  - Mobile speed up to 500 km/h.

  - Develop a methodology considering that model extensions to D2D and V2V may be developed in future SI.

- Support large antenna arrays

7 Channel model(s) for 0.5-100 GHz

7.1 Coordinate system

7.1.1 Definition

A coordinate system is defined by the x, y, z axes, the spherical angles and the spherical unit vectors as shown in Figure 7.1.1. Figure 7.1.1 defines the zenith angle θ and the azimuth angle ϕ in a Cartesian coordinate system. Note that

$\theta = 0$ points to the zenith and $\theta = 90^0$ points to the horizon. The field component in the direction of $\hat{\theta}$ is given by F_θ and the field component in the direction of $\hat{\phi}$ is given by F_ϕ.
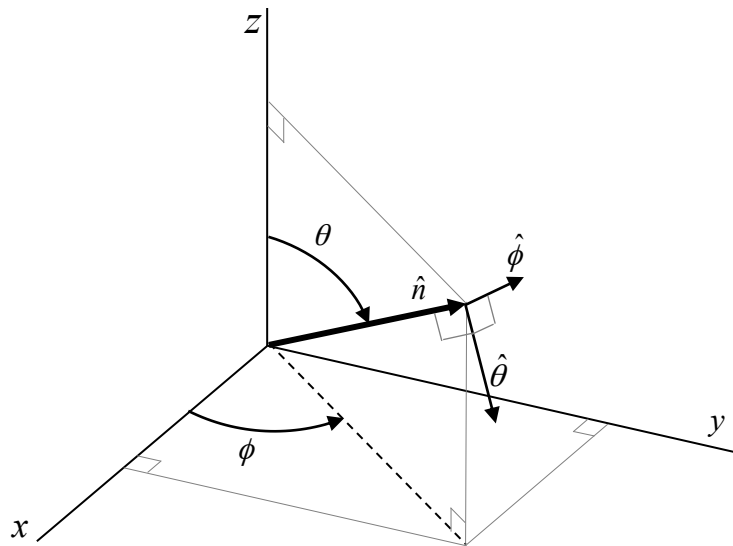
Figure 7.1.1: Definition of spherical angles and spherical unit vectors in a Cartesian coordinate system, where $\hat{n}$ is the given direction, $\hat{\theta}$ and $\hat{\phi}$ are the spherical basis vectors

7.1.2   Local and global coordinate systems

A Global Coordinate System (GCS) is defined for a system comprising multiple BSs and UTs. An array antenna for a BS or a UT can be defined in a Local Coordinate System (LCS). An LCS is used as a reference to define the vector far-field that is pattern and polarization, of each antenna element in an array. It is assumed that the far-field is known in the LCS by formulae. The placement of an array within the GCS is defined by the translation between the GCS and a LCS. The orientation of the array with respect to the GCS is defined in general by a sequence of rotations (described in clause 7.1.3). Since this orientation is in general different from the GCS orientation, it is necessary to map the vector fields of the array elements from the LCS to the GCS. This mapping depends only on the orientation of the array and is given by the equations in clause 7.1.3. Note that any arbitrary mechanical orientation of the array can be achieved by rotating the LCS with respect to the GCS.

7.1.3   Transformation from a LCS to a GCS

A GCS with coordinates (x, y, z, θ, ϕ) and unit vectors ($\hat{\theta}, \hat{\phi}$) and an LCS with "primed" coordinates ($x', y', z', \theta', \phi'$) and "primed" unit vectors ($\hat{\theta}', \hat{\phi}'$) are defined with a common origins in Figures 7.1.3-1 and 7.1.3-2. Figure 7.1.3-1 illustrates the sequence of rotations that relate the GCS (gray) and the LCS (blue). Figure 7.1.3-2 shows the coordinate direction and unit vectors of the GCS (gray) and the LCS (blue). Note that the vector fields of the array antenna elements are defined in the LCS. In Figure 7.1.3-1 we consider an arbitrary 3D-rotation of the LCS with respect to the GCS given by the angles α, β, γ. The set of angles α, β, γ can also be termed as the orientation of the array antenna with respect to the GCS.

Note that the transformation from a LCS to a GCS depends only on the angles α, β, γ. The angle α is called the bearing angle, β is called the downtilt angle and γ is called the slant angle.
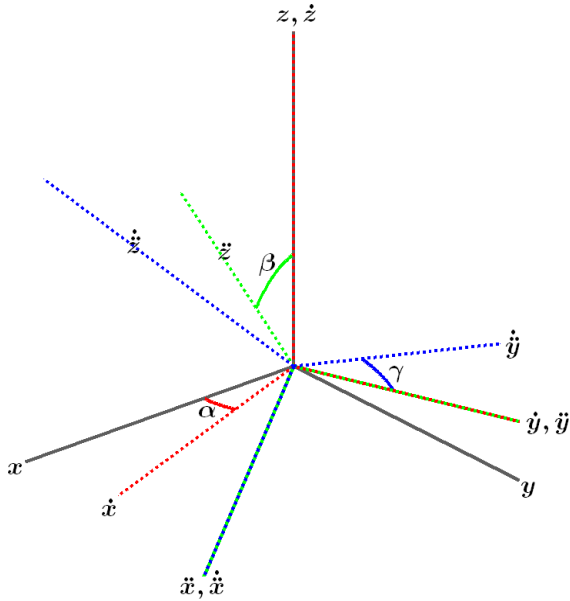
Figure 7.1.3-1: Orienting the LCS (blue) with respect to the GCS (gray) by a sequence of 3 rotations: α, β, γ.
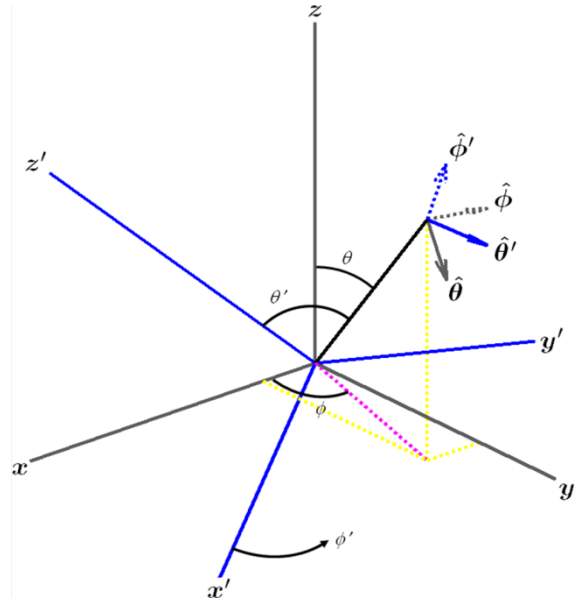
Figure 7.1.3-2: Definition of spherical coordinates and unit vectors in both the GCS and LCS.

Let $A'(\theta',\phi')$ denote an antenna element pattern in the LCS and $A(\theta,\phi)$ denote the same antenna element pattern in the GCS. Then the two are related simply by

$$A(\theta,\phi) = A'(\theta',\phi') \qquad (7.1\text{-}1)$$

with θ' and ϕ' given by (7.1-7) and (7.1-8).

Let us denote the polarized field components in the LCS by $F'_{\theta'}(\theta',\phi')$, $F'_{\phi'}(\theta',\phi')$ and in the GCS by $F_\theta(\theta,\phi)$, $F_\phi(\theta,\phi)$. Then they are related by equation (7.1-11).

Any arbitrary 3D rotation can be specified by at most 3 elemental rotations, and following the framework of Figure 7.1.3-1, a series of rotations about the z, $\dot{y}$ and $\ddot{x}$ axes are assumed here, in that order. The dotted and double-dotted marks indicate that the rotations are intrinsic, which means that they are the result of one ($\cdot$) or two ($\cdot\cdot$) intermediate rotations. In other words, the $\dot{y}$ axis is the original y axis after the first rotation about z, and the $\ddot{x}$ axis is the original x axis after the first rotation about z and the second rotation about $\dot{y}$. A first rotation of α about z sets the antenna bearing angle (i.e. the sector pointing direction for a BS antenna element). The second rotation of β about $\dot{y}$ sets the antenna downtilt angle. Finally, the third rotation of γ about $\ddot{x}$ sets the antenna slant angle. The orientation of the x, y and z axes after all three rotations can be denoted as $\dddot{x}$, $\dddot{y}$ and $\dddot{z}$. These triple-dotted axes represents the final orientation of the LCS, and for notational purposes denoted as the x', y' and z' axes (local or "primed" coordinate system).

In order to establish the equations for transformation of the coordinate system and the polarized antenna field patterns between the GCS and the LCS, it is necessary to determine the composite rotation matrix that describes the transformation of point (x, y, z) in the GCS into point (x', y', z') in the LCS. This rotation matrix is computed as the product of three elemental rotation matrices. The matrix to describe rotations about the z, $\dot{y}$ and $\ddot{x}$ axes by the angles α, β and γ respectively and in that order is defined as

$$R = R_Z(\alpha)R_Y(\beta)R_X(\gamma) = \begin{pmatrix} +\cos\alpha & -\sin\alpha & 0 \\ +\sin\alpha & +\cos\alpha & 0 \\ 0 & 0 & 1 \end{pmatrix} \begin{pmatrix} +\cos\beta & 0 & +\sin\beta \\ 0 & 1 & 0 \\ -\sin\beta & 0 & +\cos\beta \end{pmatrix} \begin{pmatrix} 1 & 0 & 0 \\ 0 & +\cos\gamma & -\sin\gamma \\ 0 & +\sin\gamma & +\cos\gamma \end{pmatrix} \qquad (7.1\text{-}2)$$

The reverse transformation is given by the inverse of R, which is also equal to the transpose of R since it is orthogonal.

$$R^{-1} = R_X(-\gamma)R_Y(-\beta)R_Z(-\alpha) = R^T \tag{7.1-3}$$

The simplified forward and reverse composite rotation matrices are given by

$$R = \begin{pmatrix} \cos\alpha\cos\beta & \cos\alpha\sin\beta\sin\gamma - \sin\alpha\cos\gamma & \cos\alpha\sin\beta\cos\gamma + \sin\alpha\sin\gamma \\ \sin\alpha\cos\beta & \sin\alpha\sin\beta\sin\gamma + \cos\alpha\cos\gamma & \sin\alpha\sin\beta\cos\gamma - \cos\alpha\sin\gamma \\ -\sin\beta & \cos\beta\sin\gamma & \cos\beta\cos\gamma \end{pmatrix} \tag{7.1-4}$$

and

$$R^{-1} = \begin{pmatrix} \cos\alpha\cos\beta & \sin\alpha\cos\beta & -\sin\beta \\ \cos\alpha\sin\beta\sin\gamma - \sin\alpha\cos\gamma & \sin\alpha\sin\beta\sin\gamma + \cos\alpha\cos\gamma & \cos\beta\sin\gamma \\ \cos\alpha\sin\beta\cos\gamma + \sin\alpha\sin\gamma & \sin\alpha\sin\beta\cos\gamma - \cos\alpha\sin\gamma & \cos\beta\cos\gamma \end{pmatrix} \tag{7.1-5}$$

These transformations can be used to derive the angular and polarization relationships between the two coordinate systems.

In order to establish the angular relationships, consider a point (x, y, z) on the unit sphere defined by the spherical coordinates $(\rho=1, \theta, \phi)$, where ρ is the unit radius, θ is the zenith angle measured from the $+z$-axis, and ϕ is the azimuth angle measured from the $+x$-axis in the x-y plane. The Cartesian representation of that point is given by

$$\hat{\rho} = \begin{pmatrix} x \\ y \\ z \end{pmatrix} = \begin{pmatrix} \sin\theta\cos\phi \\ \sin\theta\sin\phi \\ \cos\theta \end{pmatrix} \tag{7.1-6}$$

The zenith angle is computed as $\arccos(\hat{\rho}\cdot\hat{z})$ and the azimuth angle as $\arg(\hat{x}\cdot\hat{\rho} + j\,\hat{y}\cdot\hat{\rho})$, where $\hat{x}$, $\hat{y}$ and $\hat{z}$ are the Cartesian unit vectors. If this point represents a location in the GCS defined by θ and ϕ, the corresponding position in the LCS is given by $R^{-1}\hat{\rho}$, from which local angles θ' and ϕ' can be computed. The results are given in equations (7.1-7) and (7.1-8).

$$\theta'(\alpha,\beta,\gamma;\theta,\phi) = \arccos\left(\begin{bmatrix}0\\0\\1\end{bmatrix}^T R^{-1}\hat{\rho}\right) = a\cos\left(\cos\beta\cos\gamma\cos\theta + (\sin\beta\cos\gamma\cos(\phi-\alpha) - \sin\gamma\sin(\phi-\alpha))\sin\theta\right) \tag{7.1-7}$$

$$\phi'(\alpha,\beta,\gamma;\theta,\phi) = \arg\left(\begin{bmatrix}1\\j\\0\end{bmatrix}^T R^{-1}\hat{\rho}\right) = \arg\left(\begin{matrix}(\cos\beta\sin\theta\cos(\phi-\alpha) - \sin\beta\cos\theta) + \\ j(\cos\beta\sin\gamma\cos\theta + (\sin\beta\sin\gamma\cos(\phi-\alpha) + \cos\gamma\sin(\phi-\alpha))\sin\theta)\end{matrix}\right) \tag{7.1-8}$$

These formulae relate the spherical angles (θ, ϕ) of the GCS to the spherical angles (θ', ϕ') of the LCS given the rotation operation defined by the angles (α, β, γ).

Let us denote the polarized field components $F_\theta(\theta,\phi)$, $F_\phi(\theta,\phi)$ in the GCS and $F'_{\theta'}(\theta',\phi')$, $F'_{\phi'}(\theta',\phi')$ in the LCS. These are related by

$$\begin{pmatrix} F_\theta(\theta,\phi) \\ F_\phi(\theta,\phi) \end{pmatrix} = \begin{pmatrix} \hat{\theta}(\theta,\phi)^T R\hat{\theta}'(\theta',\phi') & \hat{\theta}(\theta,\phi)^T R\hat{\phi}'(\theta',\phi') \\ \hat{\phi}(\theta,\phi)^T R\hat{\theta}'(\theta',\phi') & \hat{\phi}(\theta,\phi)^T R\hat{\phi}'(\theta',\phi') \end{pmatrix} \begin{pmatrix} F'_{\theta'}(\theta',\phi') \\ F'_{\phi'}(\theta',\phi') \end{pmatrix} \tag{7.1-9}$$

In this equation, $\hat{\theta}$ and $\hat{\phi}$ represent the spherical unit vectors of the GCS, and $\hat{\theta}'$ and $\hat{\phi}'$ are the representations in the LCS. The forward rotation matrix R transforms the LCS unit vectors into the GCS frame of reference. These pairs of unit vectors are orthogonal and can be represented as shown in Figure 7.1.3-3.
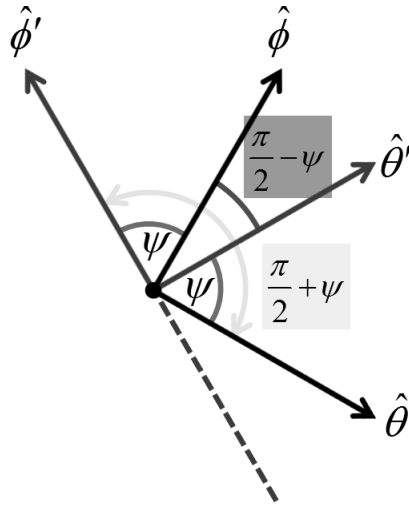
Figure 7.1.3-3: Rotation of the spherical basis vectors by an angle ψ due to the orientation of the LCS with respect to the GCS

Assuming an angular displacement of ψ between the two pairs of unit vectors, the rotation matrix of equation (7.1-9) can be further simplified as:

$$\begin{pmatrix} \hat{\theta}(\theta,\phi)^T R\hat{\theta}'(\theta',\phi') & \hat{\theta}(\theta,\phi)^T R\hat{\phi}'(\theta',\phi') \\ \hat{\phi}(\theta,\phi)^T R\hat{\theta}'(\theta',\phi') & \hat{\phi}(\theta,\phi)^T R\hat{\phi}'(\theta',\phi') \end{pmatrix} = \begin{pmatrix} \cos\psi & \cos(\pi/2+\psi) \\ \cos(\pi/2-\psi) & \cos\psi \end{pmatrix} = \begin{pmatrix} +\cos\psi & -\sin\psi \\ +\sin\psi & +\cos\psi \end{pmatrix}$$

(7.1-10)

and equation (7.1-9) can be written as:

$$\begin{pmatrix} F_\theta(\theta,\phi) \\ F_\phi(\theta,\phi) \end{pmatrix} = \begin{pmatrix} +\cos\psi & -\sin\psi \\ +\sin\psi & +\cos\psi \end{pmatrix} \begin{pmatrix} F'_{\theta'}(\theta',\phi') \\ F'_{\phi'}(\theta',\phi') \end{pmatrix}$$

(7.1-11)

The angle ψ can be computed in numerous ways from equation (7.1-10), with one such way approach being

$$\psi = \arg\left(\hat{\theta}(\theta,\phi)^T R\hat{\theta}'(\theta',\phi') + j\hat{\phi}(\theta,\phi)^T R\hat{\theta}'(\theta',\phi')\right)$$

(7.1-12)

The dot products are readily computed using the Cartesian representation of the spherical unit vectors. The general expressions for these unit vectors are given by

$$\hat{\theta} = \begin{pmatrix} \cos\theta\cos\phi \\ \cos\theta\sin\phi \\ -\sin\theta \end{pmatrix}$$

(7.1-13)

and

$$\hat{\phi} = \begin{pmatrix} -\sin\phi \\ +\cos\phi \\ 0 \end{pmatrix}$$

(7.1-14)

The angle ψ can be expressed as a function of mechanical orientation (α, β, γ) and spherical position (θ, ϕ), and is given by

$$\psi = \arg\left(\begin{array}{c}\left(\sin\gamma\cos\theta\sin(\phi-\alpha)+\cos\gamma(\cos\beta\sin\theta-\sin\beta\cos\theta\cos(\phi-\alpha))\right)+\\ j\left(\sin\gamma\cos(\phi-\alpha)+\sin\beta\cos\gamma\sin(\phi-\alpha)\right)\end{array}\right) \tag{7.1-15}$$

It can be shown that $\cos\psi$ and $\sin\psi$ can be expressed as:

$$\cos\psi = \frac{\cos\beta\cos\gamma\sin\theta-(\sin\beta\cos\gamma\cos(\phi-\alpha)-\sin\gamma\sin(\phi-\alpha))\cos\theta}{\sqrt{1-(\cos\beta\cos\gamma\cos\theta+(\sin\beta\cos\gamma\cos(\phi-\alpha)-\sin\gamma\sin(\phi-\alpha))\sin\theta)^2}} \tag{7.1-16}$$

$$\sin\psi = \frac{\sin\beta\cos\gamma\sin(\phi-\alpha)+\sin\gamma\cos(\phi-\alpha)}{\sqrt{1-(\cos\beta\cos\gamma\cos\theta+(\sin\beta\cos\gamma\cos(\phi-\alpha)-\sin\gamma\sin(\phi-\alpha))\sin\theta)^2}} \tag{7.1-17}$$

7.1.4   Transformation from an LCS to a GCS for downtilt angle only

In this clause equations are provided for the transformation from LCS to GCS assuming that the orientation of the LCS (with respect to the GCS) is such that the bearing angle α=0, the downtilt angle β is non-zero and the slant angle γ=0. In other words the y'-axis of the LCS is parallel to the y-axis of the GCS. Considering a BS antenna element the x-axis of the GCS is aligned with the pointing direction of the sector. Mechanical downtilt is modelled as a rotation of the LCS around the y-axis. For zero mechanical downtilt the LCS coincides with the GCS.

This transformation relates the spherical angles (θ,ϕ) in the global coordinate system to spherical angles (θ',ϕ') in the local (antenna-fixed) coordinate system and is defined as follows:

$$\theta' = \arccos(\cos\phi\sin\theta\sin\beta+\cos\theta\cos\beta) \tag{7.1-18}$$

$$\phi' = \arg(\cos\phi\sin\theta\cos\beta-\cos\theta\sin\beta+j\sin\phi\sin\theta) \tag{7.1-19}$$

where β is the mechanical tilt angle around the y-axis as defined in Figure 7.1.4. Note that the equations (7.1-7), (7.1-8) reduce to equations (7.1-18), (7.1-19) if both α and γ are zero.

The antenna element pattern $A(\theta,\phi)$ in the GCS is related to the antenna element pattern $A'(\theta',\phi')$ in the LCS by the relation

$$A(\theta,\phi) = A'(\theta',\phi') \tag{7.1-20}$$

with θ' and ϕ' given by (7.1-18) and (7.1-19).
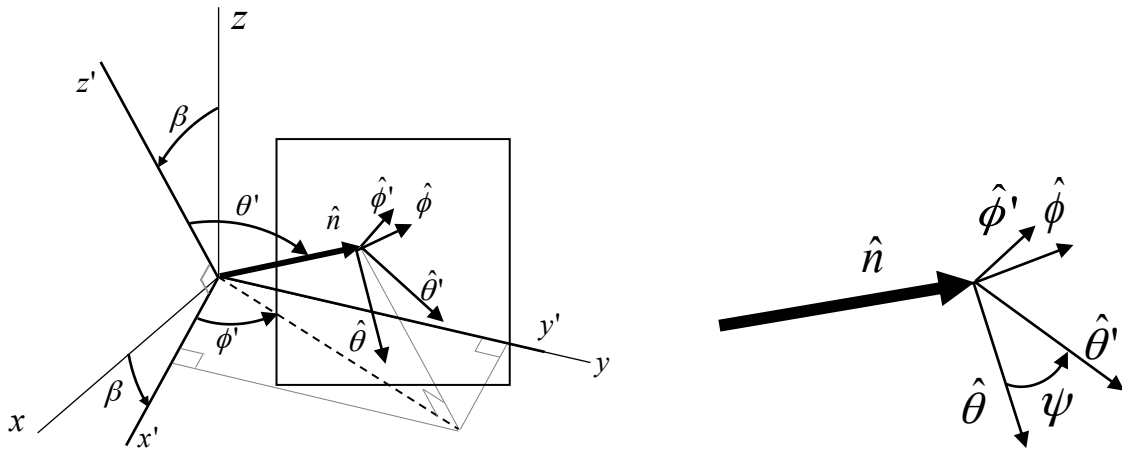
Figure 7.1.4: Definition of angles and unit vectors when the LCS has been rotated an angle β around the *y*-axis of the GCS

For a mechanical tilt angle β, the global coordinate system field components $F_\theta(\theta,\phi)$ and $F_\phi(\theta,\phi)$, are calculated from the field components $F'_{\theta'}(\theta',\phi')$ and $F'_{\phi'}(\theta',\phi')$ of the radiation pattern in the local (antenna-fixed) coordinate system as:

$$F_\theta(\theta,\phi) = F'_{\theta'}(\theta',\phi')\cos\psi - F'_{\phi'}(\theta',\phi')\sin\psi \qquad (7.1\text{-}21)$$

$$F_\phi(\theta,\phi) = F'_{\theta'}(\theta',\phi')\sin\psi + F'_{\phi'}(\theta',\phi')\cos\psi \qquad (7.1\text{-}22)$$

where θ' and ϕ' are defined as in (7.1-18) and (7.1-19), and ψ is defined as:

$$\psi = \arg\!\left(\sin\theta\cos\beta - \cos\phi\cos\theta\sin\beta + j\sin\phi\sin\beta\right). \qquad (7.1\text{-}23)$$

Note that the equation (7.1-15) is reduced to equation (7.1-23) if both α and γ are zero.

As an example, in the horizontal cut, i.e., for $\theta = 90°$, equations (7.1-18), (7.1-19) and (7.1-23) become

$$\theta' = \arccos\!\left(\cos\phi\sin\beta\right) \qquad (7.1\text{-}24)$$

$$\phi' = \arg\!\left(\cos\phi\cos\beta + j\sin\phi\right) \qquad (7.1\text{-}25)$$

$$\psi = \arg\!\left(\cos\beta + j\sin\phi\sin\beta\right) \qquad (7.1\text{-}26)$$

7.2 Scenarios

The detailed scenario description in this clause can be used for channel model calibration.

UMi-street canyon and UMa

Details on UMi-street canyon and UMa scenarios are listed in Table 7.2-1.

Table 7.2-1: Evaluation parameters for UMi-street canyon and UMa scenarios

Parameters		UMi - street canyon	UMa
Cell layout		Hexagonal grid, 19 micro sites, 3 sectors per site (ISD = 200m)	Hexagonal grid, 19 macro sites, 3 sectors per site (ISD = 500m)
BS antenna height h_{BS}		10m	25m
UT location	Outdoor/indoor	Outdoor and indoor	Outdoor and indoor
	LOS/NLOS	LOS and NLOS	LOS and NLOS
	Height h_{UT}	Same as 3D-UMi in TR36.873	Same as 3D-UMa in TR36.873
Indoor UT ratio		80%	80%
UT mobility (horizontal plane only)		3km/h	3km/h
Min. BS - UT distance (2D)		10m	35m
UT distribution (horizontal)		Uniform	Uniform

Indoor-office

Details on indoor-office scenarios are listed in Table 7.2-2 and presented in Figure 7.2-1. More details, if necessary, can be added to Figure 7.2-1.

Table 7.2-2: Evaluation parameters for indoor-office scenarios

Parameters		Indoor - office open office	Indoor - office mixed office
Layout	Room size (WxLxH)	120mx50mx3m	
	ISD	20m	
BS antenna height h_{BS}		3 m (ceiling)	
UT location	LOS/NLOS	LOS and NLOS	
	Height h_{UT}	1 m	
UT mobility (horizontal plane only)		3 km/h	
Min. BS - UT distance (2D)		0	
UT distribution (horizontal)		Uniform	

Note: The only difference between the open office and mixed office models in this TR is the line of sight probability.
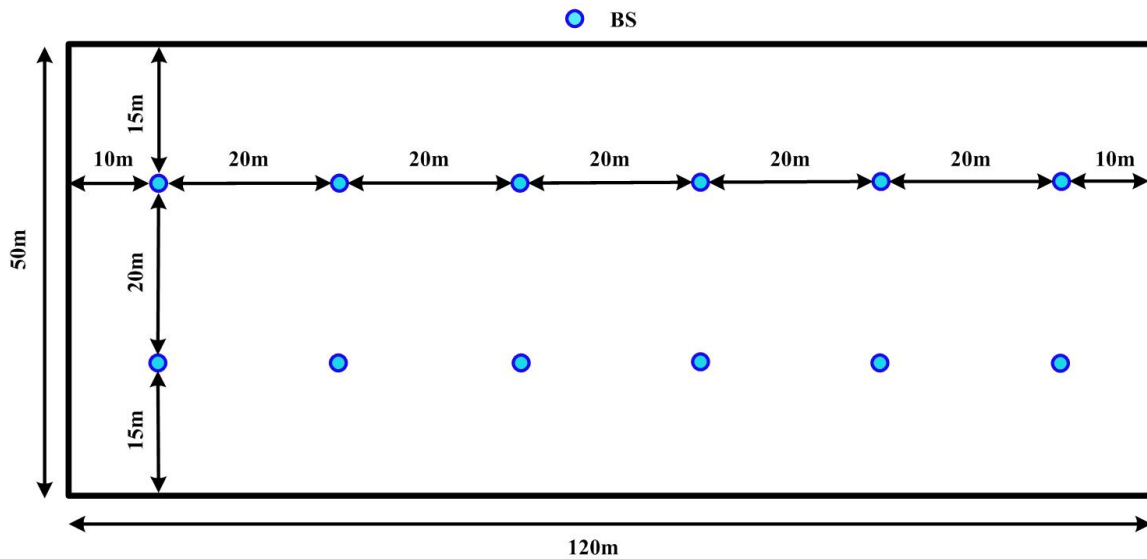
Figure 7.2-1: Layout of indoor office scenarios.

RMa

The rural deployment scenario focuses on larger and continuous coverage. The key characteristics of this scenario are continuous wide area coverage supporting high speed vehicles. This scenario will be noise-limited and/or interference-limited, using macro TRPs. Details of RMa scenario is described in Table 7.2-3.

Table 7.2-3: Evaluation parameters for RMa

Parameters	RMa
Carrier Frequency	Up to 7Ghz
BS height h_{BS}	35m
Layout	Hexagonal grid, 19 Macro sites, 3sectors per site, ISD = 1732m or 5000m
UT height h_{UT}	1.5m
UT distribution	Uniform
Indoor/Outdoor	50% indoor and 50% in car
LOS/NLOS	LOS and NLOS
Min BS - UT distance(2D)	35m

Indoor Factory (InF)

The indoor factory (InF) scenario focuses on factory halls of varying sizes and with varying levels of density of "clutter", e.g. machinery, assembly lines, storage shelves, etc. Details of the InF scenario are listed in Table 7.2-4.

Table 7.2-4: Evaluation parameters for InF

		InF				
Parameters		**InF-SL (sparse clutter, low BS)**	**InF-DL (dense clutter, low BS)**	**InF-SH (sparse clutter, high BS)**	**InF-DH (dense clutter, high BS)**	**InF-HH (high Tx, high Rx)**
Layout	Room size	Rectangular: 20-160000 m^2				
	Ceiling height	5-25 m	5-15 m	5-25 m	5-15 m	5-25 m
	Effective clutter height h_c	< Ceiling height, 0-10 m				

	External wall and ceiling type	Concrete or metal walls and ceiling with metal-coated windows				
Clutter type		Big machineries composed of regular metallic surfaces. For example: several mixed production areas with open spaces and storage/commiss ioning areas	Small to medium metallic machinery and objects with irregular structure. For example: assembly and production lines surrounded by mixed small-sized machineries.	Big machineries composed of regular metallic surfaces. For example: several mixed production areas with open spaces and storage/commissio ning areas	Small to medium metallic machinery and objects with irregular structure. For example: assembly and production lines surrounded by mixed small-sized machineries.	Any
Typical clutter size, $d_{clutter}$		10 m	2 m	10 m	2 m	Any
Clutter density r (percentage of surface area occupied by clutter)		Low clutter density (<40%)	High clutter density (≥40%)	Low clutter density (<40%)	High clutter density (≥40%)	Any
BS antenna height h_{BS}		Clutter-embedded, i.e. the BS antenna height is below the average clutter height		Above clutter		Above clutter
UT location	LOS/NLOS	LOS and NLOS				100% LOS
	Height h_{UT}	Clutter-embedded				Above clutter

7.3 Antenna modelling

This clause captures the antenna array structures considered in this SI for calibration.

The BS antenna is modelled by a uniform rectangular panel array, comprising $M_g N_g$ panels, as illustrated in Figure 7.3-1 with M_g being the number of panels in a column and N_g being the number of panels in a row. Furthermore the following properties apply:

- Antenna panels are uniformly spaced in the horizontal direction with a spacing of $d_{g,H}$ and in the vertical direction with a spacing of $d_{g,V}$.

- On each antenna panel, antenna elements are placed in the vertical and horizontal direction, where N is the number of columns, M is the number of antenna elements with the same polarization in each column.

  - Antenna numbering on the panel illustrated in Figure 7.3-1 assumes observation of the antenna array from the front (with x-axis pointing towards broad-side and increasing y-coordinate for increasing column number).

  - The antenna elements are uniformly spaced in the horizontal direction with a spacing of d_H and in the vertical direction with a spacing of d_V.

  - The antenna panel is either single polarized (P =1) or dual polarized (P =2).

The rectangular panel array antenna can be described by the following tuple $\left(M_g, N_g, M, N, P\right)$.
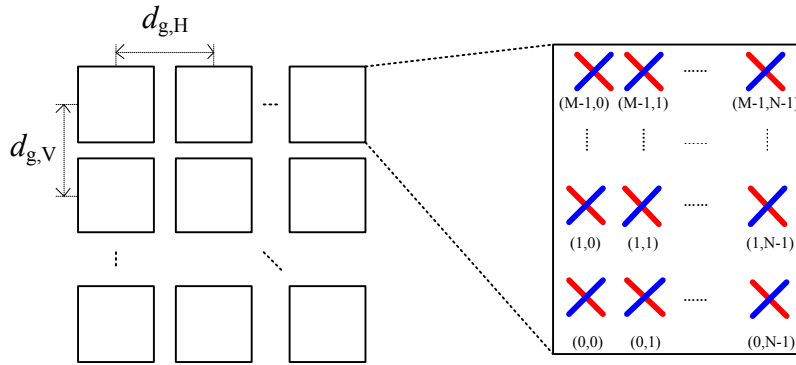
Figure 7.3-1: Cross-polarized panel array antenna model

The antenna radiation power pattern of each antenna element is generated according to Table 7.3-1.

Table 7.3-1: Radiation power pattern of a single antenna element

Parameter	Values
Vertical cut of the radiation power pattern (dB)	$$A''_{dB}\left(\theta'', \phi''=0°\right) = -\min\left\{12\left(\frac{\theta''-90°}{\theta_{3dB}}\right)^2, SLA_V\right\}$$ with $\theta_{3dB}=65°$, $SLA_V=30\,\text{dB}$ and $\theta'' \in \left[0°, 180°\right]$
Horizontal cut of the radiation power pattern (dB)	$$A''_{dB}\left(\theta''=90°, \phi''\right) = -\min\left\{12\left(\frac{\phi''}{\phi_{3dB}}\right)^2, A_{max}\right\}$$ with $\phi_{3dB}=65°$, $A_{max}=30\,\text{dB}$ and $\phi'' \in \left[-180°, 180°\right]$
3D radiation power pattern (dB)	$$A''_{dB}(\theta'', \phi'') = -\min\left\{-\left(A''_{dB}\left(\theta'', \phi''=0°\right) + A''_{dB}\left(\theta''=90°, \phi''\right)\right), A_{max}\right\}$$
Maximum directional gain of an antenna element $G_{E,max}$	<mark>8 dBi</mark>

7.3.1   Antenna port mapping

Legacy BS array antennas, i.e. uniform linear arrays with fix phase shifts between its *M* elements to obtain a beamtilt in vertical direction are modelled using complex weights

$$w_m = \frac{1}{\sqrt{M}}\exp\left(-j\frac{2\pi}{\lambda}(m-1)d_V\cos\theta_{etilt}\right) \tag{7.3-1}$$

where *m=1, ..., M*, θ_{etilt} is the electrical vertical steering angle defined between 0° and 180° (90° represents perpendicular to the array). λ denotes the wavelength and d_V the vertical element spacing.

7.3.2   Polarized antenna modelling

In general the relationship between radiation field and power pattern is given by:

$$A''(\theta'', \phi'') = \left|F''_{\theta''}\left(\theta'', \phi''\right)\right|^2 + \left|F''_{\phi''}\left(\theta'', \phi''\right)\right|^2. \tag{7.3-2}$$

The following two models represent two options on how to determine the radiation field patterns based on a defined radiation power pattern.

Model-1:

In case of polarized antenna elements assume ζ is the polarization slant angle where $\zeta = 0$ degrees corresponds to a purely vertically polarized antenna element and $\zeta = +/- 45$ degrees correspond to a pair of cross-polarized antenna elements. Then the antenna element field components in θ' and ϕ' direction are given by

$$\begin{pmatrix} F'_{\theta'}(\theta',\phi') \\ F'_{\phi'}(\theta',\phi') \end{pmatrix} = \begin{pmatrix} +\cos\psi & -\sin\psi \\ +\sin\psi & +\cos\psi \end{pmatrix} \begin{pmatrix} F''_{\theta''}(\theta'',\phi'') \\ F''_{\phi''}(\theta'',\phi'') \end{pmatrix} \qquad (7.3\text{-}3)$$

where $\cos\psi = \dfrac{\cos\zeta\sin\theta' + \sin\zeta\sin\phi'\cos\theta'}{\sqrt{1-(\cos\zeta\cos\theta' - \sin\zeta\sin\phi'\sin\theta')^2}}$, $\sin\psi = \dfrac{\sin\zeta\cos\phi'}{\sqrt{1-(\cos\zeta\cos\theta' - \sin\zeta\sin\phi'\sin\theta')^2}}$.

Note that the zenith and the azimuth field components $F'_{\theta'}(\theta',\phi')$, $F'_{\phi'}(\theta',\phi')$, $F''_{\theta''}(\theta'',\phi'')$ and $F''_{\phi''}(\theta'',\phi'')$ are defined in terms of the spherical basis vectors of an LCS as defined in Clause 7.1. The difference between the single-primed and the double-primed components is that the single-primed field components account for the polarization slant and the double-primed field components do not. For a single polarized antenna (purely vertically polarized antenna) we can write $F''_{\theta''}(\theta'',\phi'') = \sqrt{A''(\theta'',\phi'')}$ and $F''_{\phi''}(\theta'',\phi'') = 0$ where $A''(\theta'',\phi'')$ is the 3D antenna radiation power pattern as a function of azimuth angle ϕ'' and zenith angle θ'' in the LCS as defined in Table 7.3-1 converted into linear scale.

Model-2:

In case of polarized antennas, the polarization is modelled as angle-independent in both azimuth and elevation, in an LCS. For a linearly polarized antenna, the antenna element field pattern, in the vertical polarization and in the horizontal polarization, are given by

$$F'_{\theta'}(\theta',\phi') = \sqrt{A'(\theta',\phi')}\cos(\zeta) \qquad (7.3\text{-}4)$$

and

$$F'_{\phi'}(\theta',\phi') = \sqrt{A'(\theta',\phi')}\sin(\zeta), \qquad (7.3\text{-}5)$$

respectively, where ζ is the polarization slant angle and $A'(\theta',\phi')$ is the 3D antenna element power pattern as a function of azimuth angle, ϕ' and elevation angle, θ' in the LCS. Note that $\zeta = 0$ degrees correspond to a purely vertically polarized antenna element. The vertical and horizontal field directions are defined in terms of the spherical basis vectors, $\hat{\theta}'$ and $\hat{\phi}'$ respectively in the LCS as defined in Clause 7.1.2. Also $A'(\theta',\phi') = A''(\theta'',\phi'')$, $\theta' = \theta''$ and $\phi' = \phi''$ as defined in Table 7.1-1.

7.4 Pathloss, LOS probability and penetration modelling

7.4.1 Pathloss

The pathloss models are summarized in Table 7.4.1-1 and the distance definitions are indicated in Figure 7.4.1-1 and Figure 7.4.1-2. Note that the distribution of the shadow fading is log-normal, and its standard deviation for each scenario is given in Table 7.4.1-1.
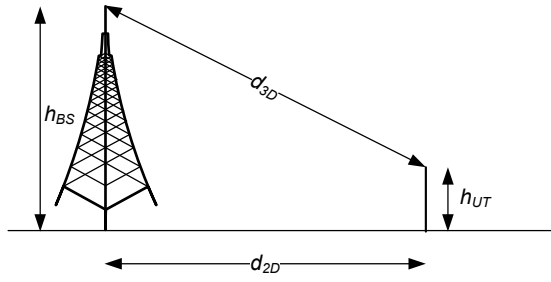
Figure7.4.1-1: Definition of d_{2D} and d_{3D} for outdoor UTs
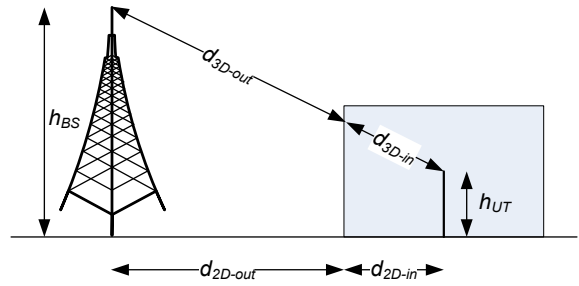
Figure 7.4.1-2: Definition of d_{2D-out}, d_{2D-in} and d_{3D-out}, d_{3D-in} for indoor UTs.

Note that

$$d_{3D-out} + d_{3D-in} = \sqrt{\left(d_{2D-out} + d_{2D-in}\right)^2 + \left(h_{BS} - h_{UT}\right)^2} \qquad (7.4\text{-}1)$$

Table 7.4.1-1: Pathloss models

Scenario	LOS/NLOS	Pathloss [dB], f_c is in GHz and d is in meters, see note 6	Shadow fading std [dB]	Applicability range, antenna height default values
RMa	LOS	$PL_{\text{RMa-LOS}} = \begin{cases} PL_1 & 10\text{m} \le d_{2D} \le d_{BP} \\ PL_2 & d_{BP} \le d_{2D} \le 10\text{km} \end{cases}$, see note 5 $PL_1 = 20\log_{10}(40\pi d_{3D} f_c / 3) + \min(0.03 h^{1.72}, 10)\log_{10}(d_{3D})$ $\quad - \min(0.044 h^{1.72}, 14.77) + 0.002\log_{10}(h) d_{3D}$ $PL_2 = PL_1(d_{BP}) + 40\log_{10}(d_{3D}/d_{BP})$	$\sigma_{SF} = 4$ $\sigma_{SF} = 6$	$h_{BS} = 35\text{m}$ $h_{UT} = 1.5\text{m}$ $W = 20\text{m}$ $h = 5\text{m}$ h = avg. building height W = avg. street width The applicability ranges: $5\text{m} \le h \le 50\text{m}$ $5\text{m} \le W \le 50\text{m}$ $10\text{m} \le h_{BS} \le 150\text{m}$ $1\text{m} \le h_{UT} \le 10\text{m}$
	NLOS	$PL_{\text{RMa-NLOS}} = \max(PL_{\text{RMa-LOS}}, PL'_{\text{RMa-NLOS}})$ $\quad$ for $10\text{m} \le d_{2D} \le 5\text{km}$ $PL'_{\text{RMa-NLOS}} = 161.04 - 7.1\log_{10}(W) + 7.5\log_{10}(h)$ $\quad - (24.37 - 3.7(h/h_{BS})^2)\log_{10}(h_{BS})$ $\quad + (43.42 - 3.1\log_{10}(h_{BS}))(\log_{10}(d_{3D}) - 3)$ $\quad + 20\log_{10}(f_c) - (3.2(\log_{10}(11.75 h_{UT}))^2 - 4.97)$	$\sigma_{SF} = 8$	
UMa	LOS	$PL_{\text{UMa-LOS}} = \begin{cases} PL_1 & 10\text{m} \le d_{2D} \le d'_{BP} \\ PL_2 & d'_{BP} \le d_{2D} \le 5\text{km} \end{cases}$, see note 1 $PL_1 = 28.0 + 22\log_{10}(d_{3D}) + 20\log_{10}(f_c)$ $PL_2 = 28.0 + 40\log_{10}(d_{3D}) + 20\log_{10}(f_c)$ $\quad - 9\log_{10}((d'_{BP})^2 + (h_{BS} - h_{UT})^2)$	$\sigma_{SF} = 4$	$1.5\text{m} \le h_{UT} \le 22.5\text{m}$ $h_{BS} = 25\text{m}$
	NLOS	$PL_{\text{UMa-NLOS}} = \max(PL_{\text{UMa-LOS}}, PL'_{\text{UMa-NLOS}})$ $\quad$ for $10\text{m} \le d_{2D} \le 5\text{km}$ $PL'_{\text{UMa-NLOS}} = 13.54 + 39.08\log_{10}(d_{3D}) +$ $\quad 20\log_{10}(f_c) - 0.6(h_{UT} - 1.5)$	$\sigma_{SF} = 6$	$1.5\text{m} \le h_{UT} \le 22.5\text{m}$ $h_{BS} = 25\text{m}$ Explanations: see note 3
		Optional $PL = 32.4 + 20\log_{10}(f_c) + 30\log_{10}(d_{3D})$	$\sigma_{SF} = 7.8$	
UMi - Street Canyon	LOS	$PL_{\text{UMi-LOS}} = \begin{cases} PL_1 & 10\text{m} \le d_{2D} \le d'_{BP} \\ PL_2 & d'_{BP} \le d_{2D} \le 5\text{km} \end{cases}$, see note 1 $PL_1 = 32.4 + 21\log_{10}(d_{3D}) + 20\log_{10}(f_c)$ $PL_2 = 32.4 + 40\log_{10}(d_{3D}) + 20\log_{10}(f_c)$ $\quad - 9.5\log_{10}((d'_{BP})^2 + (h_{BS} - h_{UT})^2)$	$\sigma_{SF} = 4$	$1.5\text{m} \le h_{UT} \le 22.5\text{m}$ $h_{BS} = 10\text{m}$

	NLOS	$PL_{\text{UMi-NLOS}} = \max(PL_{\text{UMi-LOS}}, PL'_{\text{UMi-NLOS}})$ for $10\text{m} \leq d_{2D} \leq 5\text{km}$ $PL'_{\text{UMi-NLOS}} = 35.3\log_{10}(d_{3D}) + 22.4$ $+ 21.3\log_{10}(f_c) - 0.3(h_{\text{UT}} - 1.5)$	$\sigma_{\text{SF}} = 7.82$	$1.5\text{m} \leq h_{\text{UT}} \leq 22.5\text{m}$ $h_{\text{BS}} = 10\text{m}$ Explanations: see note 4
		Optional $PL = 32.4 + 20\log_{10}(f_c) + 31.9\log_{10}(d_{3D})$	$\sigma_{\text{SF}} = 8.2$	
InH - Office	**LOS**	$PL_{\text{InH-LOS}} = 32.4 + 17.3\log_{10}(d_{3D}) + 20\log_{10}(f_c)$	$\sigma_{\text{SF}} = 3$	$1\text{m} \leq d_{3D} \leq 150\text{m}$
	NLOS	$PL_{\text{InH-NLOS}} = \max(PL_{\text{InH-LOS}}, PL'_{\text{InH-NLOS}})$ $PL'_{\text{InH-NLOS}} = 38.3\log_{10}(d_{3D}) + 17.30 + 24.9\log_{10}(f_c)$	$\sigma_{\text{SF}} = 8.03$	$1\text{m} \leq d_{3D} \leq 150\text{m}$
		Optional $PL'_{\text{InH-NLOS}} = 32.4 + 20\log_{10}(f_c) + 31.9\log_{10}(d_{3D})$	$\sigma_{\text{SF}} = 8.29$	$1\text{m} \leq d_{3D} \leq 150\text{m}$
InF	**LOS**	$PL_{LOS} = 31.84 + 21.50\log_{10}(d_{3D}) + 19.00\log_{10}(f_c)$	$\sigma_{SF} = 4.$	$1 \leq d_{3D} \leq 600\,m$
	NLOS	InF-SL: $PL = 33 + 25.5\log_{10}(d_{3D}) + 20\log_{10}(f_c)$ $PL_{NLOS} = \max(PL, PL_{LOS})$	$\sigma_{SF} = 5.7$	
		InF-DL: $PL = 18.6 + 35.7\log_{10}(d_{3D}) + 20\log_{10}(f_c)$ $PL_{NLOS} = \max(PL, PL_{LOS}, PL_{InF-SL})$	$\sigma_{SF} = 7.2$	
		InF-SH: $PL = 32.4 + 23.0\log_{10}(d_{3D}) + 20\log_{10}(f_c)$ $PL_{NLOS} = \max(PL, PL_{LOS})$	$\sigma_{SF} = 5.9$	
		InF-DH: $PL = 33.63 + 21.9\log_{10}(d_{3D}) + 20\log_{10}(f_c)$ $PL_{NLOS} = \max(PL, PL_{LOS})$	$\sigma_{SF} = 4.0$	

Note 1: Breakpoint distance $d'_{BP} = 4\, h'_{BS}\, h'_{UT}\, f_c/c$, where f_c is the centre frequency in Hz, $c = 3.0 \times 10^8$ m/s is the propagation velocity in free space, and h'_{BS} and h'_{UT} are the effective antenna heights at the BS and the UT, respectively. The effective antenna heights h'_{BS} and h'_{UT} are computed as follows: $h'_{BS} = h_{BS} - h_E$, $h'_{UT} = h_{UT} - h_E$, where h_{BS} and h_{UT} are the actual antenna heights, and h_E is the effective environment height. For UMi $h_E = 1.0$m. For UMa $h_E = 1$m with a probability equal to $1/(1+C(d_{2D}, h_{UT}))$ and chosen from a discrete uniform distribution uniform$(12,15,\ldots,(h_{UT}-1.5))$ otherwise. With $C(d_{2D}, h_{UT})$ given by

$$C\!\left(d_{2D}, h_{UT}\right) = \begin{cases} 0 & ,h_{UT} < 13\text{m} \\ \left(\dfrac{h_{UT} - 13}{10}\right)^{1.5} g\!\left(d_{2D}\right) & ,13\text{m} \le h_{UT} \le 23\text{m} \end{cases},$$

where

$$g\!\left(d_{2D}\right) = \begin{cases} 0 & ,d_{2D} \le 18\text{m} \\ \dfrac{5}{4}\left(\dfrac{d_{2D}}{100}\right)^{3} \exp\!\left(\dfrac{-d_{2D}}{150}\right) & ,18\text{m} < d_{2D} \end{cases}.$$

Note that h_E depends on d_{2D} and h_{UT} and thus needs to be independently determined for every link between BS sites and UTs. A BS site may be a single BS or multiple co-located BSs.

Note 2: The applicable frequency range of the PL formula in this table is $0.5 < f_c < f_H$ GHz, where $f_H = 30$ GHz for RMa and $f_H = 100$ GHz for all the other scenarios. It is noted that RMa pathloss model for >7 GHz is validated based on a single measurement campaign conducted at 24 GHz.

Note 3: UMa NLOS pathloss is from TR36.873 with simplified format and $PL_{UMa-LOS}$ = Pathloss of UMa LOS outdoor scenario.

Note 4: $PL_{UMi-LOS}$ = Pathloss of UMi-Street Canyon LOS outdoor scenario.

Note 5: Break point distance $d_{BP} = 2\pi\, h_{BS}\, h_{UT}\, f_c/c$, where f_c is the centre frequency in Hz, $c = 3.0 \times 10^8$ m/s is the propagation velocity in free space, and h_{BS} and h_{UT} are the antenna heights at the BS and the UT, respectively.

Note 6: f_c denotes the center frequency normalized by 1GHz, all distance related values are normalized by 1m, unless it is stated otherwise.

7.4.2 LOS probability

The Line-Of-Sight (LOS) probabilities are given in Table 7.4.2-1.

Table 7.4.2-1 LOS probability

Scenario	LOS probability (distance is in meters)
RMa	$$\Pr_{\text{LOS}} = \begin{cases} 1 & , d_{\text{2D-out}} \leq 10\text{m} \\ \exp\left(-\dfrac{d_{\text{2D-out}} - 10}{1000}\right) & , 10\text{m} < d_{\text{2D-out}} \end{cases}$$
UMi - Street canyon	$$\Pr_{\text{LOS}} = \begin{cases} 1 & , d_{\text{2D-out}} \leq 18\text{m} \\ \dfrac{18}{d_{\text{2D-out}}} + \exp\left(-\dfrac{d_{\text{2D-out}}}{36}\right)\left(1 - \dfrac{18}{d_{\text{2D-out}}}\right) & , 18\text{m} < d_{\text{2D-out}} \end{cases}$$
UMa	$$\Pr_{\text{LOS}} = \begin{cases} 1 & , d_{\text{2D-out}} \leq 18\text{m} \\ \left[\dfrac{18}{d_{\text{2D-out}}} + \exp\left(-\dfrac{d_{\text{2D-out}}}{63}\right)\left(1 - \dfrac{18}{d_{\text{2D-out}}}\right)\right]\left(1 + C'(h_{\text{UT}})\dfrac{5}{4}\left(\dfrac{d_{\text{2D-out}}}{100}\right)^3 \exp\left(-\dfrac{d_{\text{2D-out}}}{150}\right)\right) & , 18\text{m} < d_{\text{2D-out}} \end{cases}$$ where $$C'(h_{\text{UT}}) = \begin{cases} 0 & , h_{\text{UT}} \leq 13\text{m} \\ \left(\dfrac{h_{\text{UT}} - 13}{10}\right)^{1.5} & , 13\text{m} < h_{\text{UT}} \leq 23\text{m} \end{cases}$$
Indoor - Mixed office	$$\Pr_{\text{LOS}} = \begin{cases} 1 & , d_{\text{2D-in}} \leq 1.2\text{m} \\ \exp\left(-\dfrac{d_{\text{2D-in}} - 1.2}{4.7}\right) & , 1.2\text{m} < d_{\text{2D-in}} < 6.5\text{m} \\ \exp\left(-\dfrac{d_{\text{2D-in}} - 6.5}{32.6}\right)\cdot 0.32 & , 6.5\text{m} \leq d_{\text{2D-in}} \end{cases}$$
Indoor - Open office	$$\Pr_{\text{LOS}} = \begin{cases} 1 & , d_{\text{2D-in}} \leq 5\text{m} \\ \exp\left(-\dfrac{d_{\text{2D-in}} - 5}{70.8}\right) & , 5\text{m} < d_{\text{2D-in}} \leq 49\text{m} \\ \exp\left(-\dfrac{d_{\text{2D-in}} - 49}{211.7}\right)\cdot 0.54 & , 49\text{m} < d_{\text{2D-in}} \end{cases}$$
InF-SL InF-SH InF-DL InF-DH	$$\Pr_{\text{LOS,subsce}}(d_{\text{2D}}) = \exp\left(-\dfrac{d_{\text{2D}}}{k_{\text{subsce}}}\right)$$ where $$k_{subsce} = \begin{cases} -\dfrac{d_{clutter}}{\ln(1-r)} & \text{for InF-SL and InF-DL} \\ -\dfrac{d_{clutter}}{\ln(1-r)} \cdot \dfrac{h_{BS} - h_{UT}}{h_c - h_{UT}} & \text{for InF-SH and InF-DH} \end{cases}$$ The parameters $d_{clutter}$, r, and h_c are defined in Table 7.2-4
InF-HH	$\Pr_{\text{LOS}} = 1$
Note:	The LOS probability is derived with assuming antenna heights of 3m for indoor, 10m for UMi, and 25m for UMa

7.4.3   O2I penetration loss

7.4.3.1   O2I building penetration loss

The pathloss incorporating O2I building penetration loss is modelled as in the following:

$$PL = PL_b + PL_{tw} + PL_{in} + N(0, \sigma_P^2) \qquad (7.4-2)$$

where PL_b is the basic outdoor path loss given in Clause 7.4.1, where d_{3D} is replaced by $d_{3D-out} + d_{3D-in}$. PL_{tw} is the building penetration loss through the external wall, PL_{in} is the inside loss dependent on the depth into the building, and σ_P is the standard deviation for the penetration loss.

PL_{tw} is characterized as:

$$PL_{tw} = PL_{npi} - 10\log_{10}\sum_{i=1}^{N}\left(p_i \times 10^{\frac{L_{material\_i}}{-10}} \right) \qquad (7.4-3)$$

PL_{npi} is an additional loss is added to the external wall loss to account for non-perpendicular incidence;

$L_{material\_i} = a_{material\_i} + b_{material\_i} \cdot f$, is the penetration loss of material i, example values of which can be found in

Table 7.4.3-1; p_i is proportion of i-th materials, where $\sum_{i=1}^{N} p_i = 1$; and N is the number of materials.

Table 7.4.3-1: Material penetration losses

Material	Penetration loss [dB]
Standard multi-pane glass	$L_{glass} = 2 + 0.2f$
IRR glass	$L_{IIRglass} = 23 + 0.3f$
Concrete	$L_{concrete} = 5 + 4f$
Wood	$L_{wood} = 4.85 + 0.12f$
Note: f is in GHz	

Table 7.4.3-2 gives PL_{tw}, PL_{in} and σ_P for two O2I penetration loss models. The O2I penetration is UT-specifically generated, and is added to the SF realization in the log domain.

Table 7.4.3-2: O2I building penetration loss model

	Path loss through external wall: PL_{tw} in [dB]	Indoor loss: PL_{in} in [dB]	Standard deviation: σ_P in [dB]
Low-loss model	$5 - 10\log_{10}\left(0.3 \cdot 10^{\frac{-L_{glass}}{10}} + 0.7 \cdot 10^{\frac{-L_{concrete}}{10}} \right)$	$0.5\, d_{2D-in}$	4.4
High-loss model	$5 - 10\log_{10}\left(0.7 \cdot 10^{\frac{-L_{IIRglass}}{10}} + 0.3 \cdot 10^{\frac{-L_{concrete}}{10}} \right)$	$0.5\, d_{2D-in}$	6.5

d_{2D-in} is minimum of two independently generated uniformly distributed variables between 0 and 25 m for UMa and UMi-Street Canyon, and between 0 and 10 m for RMa. d_{2D-in} shall be UT-specifically generated.

Both low-loss and high-loss models are applicable to UMa and UMi-Street Canyon.

Only the low-loss model is applicable to RMa.

Only the high-loss model is applicable to InF.

The composition of low and high loss is a simulation parameter that should be determined by the user of the channel models, and is dependent on the use of metal-coated glass in buildings and the deployment scenarios. Such use is expected to differ in different markets and regions of the world and also may increase over years to new regulations and energy saving initiatives. Furthermore, the use of such high-loss glass currently appears to be more predominant in commercial buildings than in residential buildings in some regions of the world (see note).

   Note: One example survey for the US market can be found in [5]. The survey does not necessarily be representative for all the scenarios. Other ratios outside of the survey should not be precluded.

For backwards compatibility with TR 36.873 [3], the following building penetration model should be used for UMa and UMi single-frequency simulations at frequencies below 6 GHz.

Table 7.4.3-3. O2I building penetration loss model for single-frequency simulations <6 GHz

Parameter	Value
PL_{tw}	20 dB
PL_{in}	0.5 d_{2D-in} with d_{2D-in} being *a single, link-specific,* uniformly distributed variable between 0 and 25 m
σ_P	0 dB
σ_{SF}	7 dB (note: replacing the respective value in Table 7.4.1-1)

7.4.3.2   O2I car penetration loss

The pathloss incorporating O2I car penetration loss is modelled as in the following:

$$PL = PL_b + N(\mu, \sigma_P^2) \tag{7.4-4}$$

where PL_b is the basic outdoor path loss given in Clause 7.4.1. $\mu = 9$, and $\sigma_P = 5$. The car penetration loss shall be UT-specifically generated. Optionally, for metallized car windows, $\mu = 20$ can be used. The O2I car penetration loss models are applicable for at least 0.6-60 GHz.

7.4.4   Autocorrelation of shadow fading

The long-term (log-normal) fading in the logarithmic scale around the mean path loss *PL* (dB) is characterized by a Gaussian distribution with zero mean and standard deviation. Due to the slow fading process versus distance Δx (Δx is in the horizontal plane), adjacent fading values are correlated. Its normalized autocorrelation function $R(\Delta x)$ can be described with sufficient accuracy by the exponential function ITU-R Rec. P.1816 [18]

$$R(\Delta x) = e^{-\frac{|\Delta x|}{d_{cor}}} \tag{7.4-5}$$

with the correlation length d_{cor} being dependent on the environment, see the correlation parameters for shadowing and other large scale parameters in Table 7.5-6 (Channel model parameters). In a spatial consistency procedure in Clause 7.6.3, the cluster specific random variables are also correlated following the exponential function with respect to correlation distances in the two dimensional horizontal plane.

7.5   Fast fading model

The radio channel realizations are created using the parameters listed in Table 7.5-1. The channel realizations are obtained by a step-wise procedure illustrated in Figure 7.5-1 and described below. It has to be noted that the geometric description covers arrival angles from the last bounce scatterers and respectively departure angles to the first scatterers interacted from the transmitting side. The propagation between the first and the last interaction is not defined. Thus, this approach can model also multiple interactions with the scattering media. This indicates also that e.g., the delay of a multipath component cannot be determined by the geometry. In the following steps, downlink is assumed. For uplink, arrival and departure parameters have to be swapped.

Note: the channel generation in this clause is enough for at least the following cases.

- Case 1: For low complexity evaluations

- Case 2: To compare with earlier simulation results,

- Case 3: When none of the additional modelling components are turned on.

For other advanced simulations, e.g., spatially consistency, large bandwidth and arrays, oxygen absorption, blockage, absolute time of arrival, dual mobility, embedded devices, etc., some of the additional modelling components of Clause 7.6 should be considered.
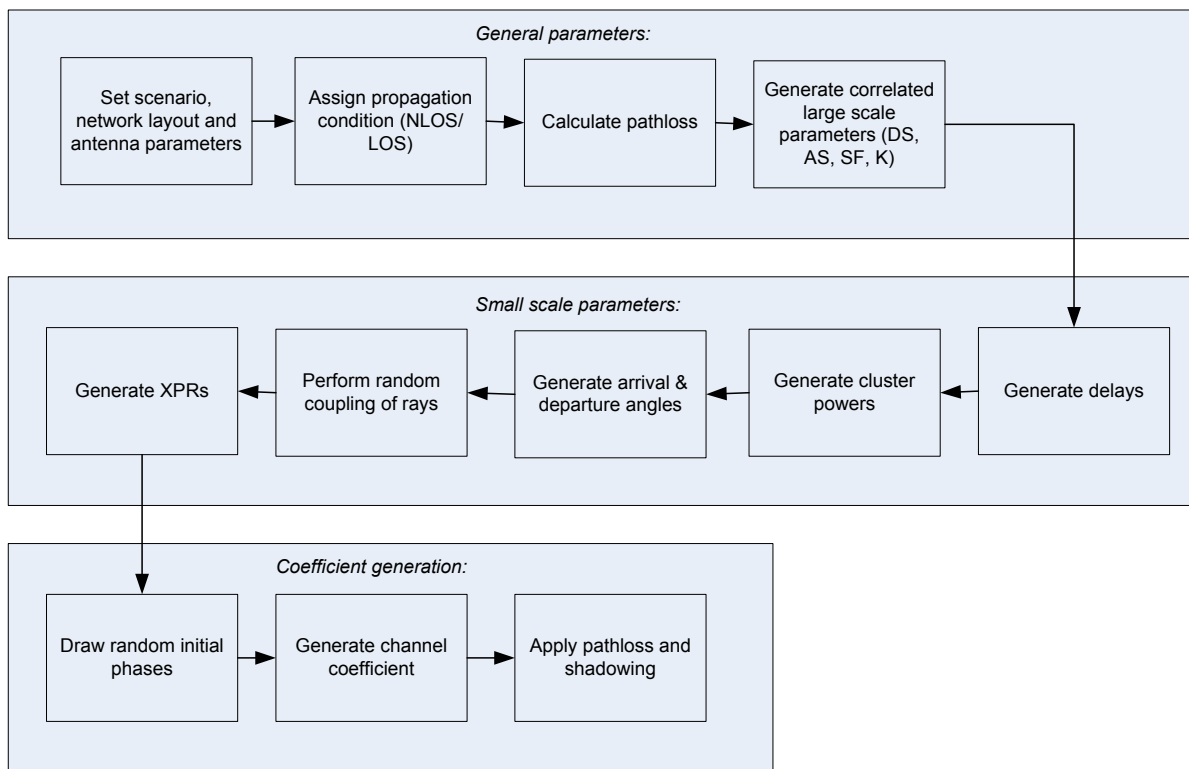
Figure 7.5-1 Channel coefficient generation procedure
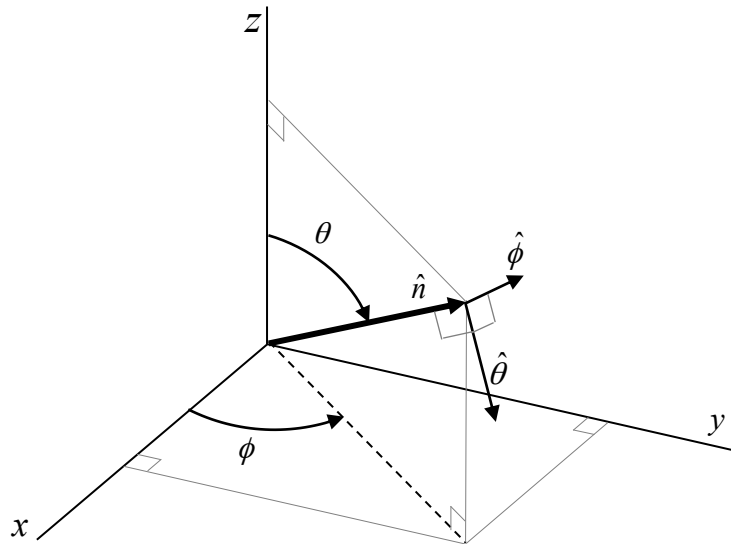
Figure 7.5-2: Definition of a global coordinate system showing the zenith angle θ and the azimuth angle ϕ. θ=0° points to zenith and θ=+90° points to the horizon.
The spherical basis vectors $\hat{\theta}$ and $\hat{\phi}$ shown above are defined based on the direction of propagation $\hat{n}$.

Table 7.5-1: Notations in the global coordinate system (GCS)

Parameter	Notation
LOS AOD	$\phi_{LOS,AOD}$
LOS AOA	$\phi_{LOS,AOA}$
LOS ZOD	$\theta_{LOS,ZOD}$
LOS ZOA	$\theta_{LOS,ZOA}$
AOA for cluster n	$\phi_{n,AOA}$
AOD for cluster n	$\phi_{n,AOD}$
AOA for ray m in cluster n	$\phi_{n,m,AOA}$
AOD for ray m in cluster n	$\phi_{n,m,AOD}$
ZOA for cluster n	$\theta_{n,ZOA}$
ZOD for cluster n	$\theta_{n,ZOD}$
ZOA for ray m in cluster n	$\theta_{n,m,ZOA}$
ZOD for ray m in cluster n	$\theta_{n,m,ZOD}$
Receive antenna element u field pattern in the direction of the spherical basis vector $\hat{\theta}$	$F_{rx,u,\theta}$
Receive antenna element u field pattern in the direction of the spherical basis vector $\hat{\phi}$	$F_{rx,u,\phi}$
Transmit antenna element s field pattern in the direction of the spherical basis vector $\hat{\theta}$	$F_{tx,s,\theta}$
Transmit antenna element s field pattern in the direction of the spherical basis vector $\hat{\phi}$	$F_{rx,s,\phi}$

Step 1: Set environment, network layout, and antenna array parameters

  a) Choose one of the scenarios (e.g. UMa, UMi-Street Canyon, RMa, InH-Office or InF). Choose a global coordinate system and define zenith angle θ, azimuth angle ϕ, and spherical basis vectors $\hat{\theta}$, $\hat{\phi}$ as shown in Figure 7.3-2. Note: Scenario RMa is for up to 7GHz while others are for up to 100GHz

  b) Give number of BS and UT

  c) Give 3D locations of BS and UT, and determine LOS AOD ($\phi_{LOS,AOD}$), LOS ZOD ($\theta_{LOS,ZOD}$), LOS AOA ($\phi_{LOS,AOA}$), and LOS ZOA ($\theta_{LOS,ZOA}$) of each BS and UT in the global coordinate system

  d) Give BS and UT antenna field patterns F_{rx} and F_{tx} in the global coordinate system and array geometries

e) Give BS and UT array orientations with respect to the global coordinate system. BS array orientation is defined by three angles $\Omega_{BS,\alpha}$ (BS bearing angle), $\Omega_{BS,\beta}$ (BS downtilt angle) and $\Omega_{BS,\gamma}$ (BS slant angle). UT array orientation is defined by three angles $\Omega_{UT,\alpha}$ (UT bearing angle), $\Omega_{UT,\beta}$ (UT downtilt angle) and $\Omega_{UT,\gamma}$ (UT slant angle).

f) Give speed and direction of motion of UT in the global coordinate system

g) Specify system centre frequency f_c and bandwidth B

Note: In case wrapping is used, each wrapping copy of a BS or site should be treated as a separate BS/site considering channel generation.

Large scale parameters:

Step 2: Assign propagation condition (LOS/NLOS) according to Table 7.4.2-1. The propagation conditions for different BS-UT links are uncorrelated.

Also, assign an indoor/outdoor state for each UT. It is noted that all the links from a UT have the same indoor/outdoor state.

Step 3: Calculate pathloss with formulas in Table 7.4.1-1 for each BS-UT link to be modelled.

Step 4: Generate large scale parameters, e.g. delay spread (DS), angular spreads (ASA, ASD, ZSA, ZSD), Ricean K factor (K) and shadow fading (SF) taking into account cross correlation according to Table 7.5-6 and using the procedure described in clause 3.3.1 of [14] with the square root matrix $\sqrt{C_{MxM}(0)}$ being generated using the Cholesky decomposition and the following order of the large scale parameter vector: $\mathbf{s}_M = [s_{SF}, s_K, s_{DS}, s_{ASD}, s_{ASA}, s_{ZSD}, s_{ZSA}]^T$.

These LSPs for different BS-UT links are uncorrelated, but the LSPs for links from co-sited sectors to a UT are the same. In addition, these LSPs for the links of UTs on different floors are uncorrelated.

Limit random RMS azimuth arrival and azimuth departure spread values to 104 degrees, i.e., ASA= min(ASA, 104°), ASD = min(ASD, 104°). Limit random RMS zenith arrival and zenith departure spread values to 52 degrees, i.e., ZSA = min(ZSA, 52°), ZSD = min(ZSD, 52°).

Small scale parameters:

Step 5: Generate cluster delays τ_n.

Delays are drawn randomly from the delay distribution defined in Table 7.5-6. With exponential delay distribution calculate

$$\tau'_n = -r_\tau \mathrm{DS}\ln(X_n), \tag{7.5-1}$$

Where r_τ is the delay distribution proportionality factor, $X_n \sim$ uniform(0,1), and cluster index $n = 1,\ldots,N$. With uniform delay distribution the delay values τ'_n are drawn from the corresponding range. Normalise the delays by subtracting the minimum delay and sort the normalised delays to ascending order:

$$\tau_n = \mathrm{sort}(\tau'_n - \min(\tau'_n)). \tag{7.5-2}$$

In the case of LOS condition, additional scaling of delays is required to compensate for the effect of LOS peak addition to the delay spread. The heuristically determined Ricean K-factor dependent scaling constant is

$$C_\tau = 0.7705 - 0.0433K + 0.0002K^2 + 0.000017K^3, \tag{7.5-3}$$

where K [dB] is the Ricean K-factor as generated in Step 4. The scaled delays

$$\tau_n^{LOS} = \tau_n / C_\tau,$$ (7.5-4)

are **not** to be used in cluster power generation.

Step 6: Generate cluster powers P_n.

Cluster powers are calculated assuming a single slope exponential power delay profile. Power assignment depends on the delay distribution defined in Table 7.5-6. With exponential delay distribution the cluster powers are determined by

$$P_n' = \exp\left(-\tau_n \frac{r_\tau - 1}{r_\tau \mathrm{DS}}\right) \cdot 10^{\frac{-Z_n}{10}}$$ (7.5-5)

where $Z_n \sim N\left(0, \xi^2\right)$ is the per cluster shadowing term in [dB]. Normalize the cluster powers so that the sum of all cluster powers is equal to one, i.e.,

$$P_n = \frac{P_n'}{\sum_{n=1}^{N} P_n'}$$ (7.5-6)

In the case of LOS condition an additional specular component is added to the first cluster. Power of the single LOS ray is:

$$P_{1,LOS} = \frac{K_R}{K_R + 1}$$ (7.5-7)

and the cluster powers are not normalized as in equation (7.5-6) , but:

$$P_n = \frac{1}{K_R + 1} \frac{P_n'}{\sum_{n=1}^{N} P_n'} + \delta(n-1)P_{1,LOS}$$ (7.5-8)

where $\delta(.)$ is Dirac's delta function and K_R is the Ricean *K*-factor as generated in Step 4 converted to linear scale. These power values are used *only* in equations (7.5-9) and (7.5-14), but *not* in equation (7.5-22).

Assign the power of each ray within a cluster as P_n / M, where *M* is the number of rays per cluster.

Remove clusters with less than -25 dB power compared to the maximum cluster power. The scaling factors need not be changed after cluster elimination.

Step 7: Generate arrival angles and departure angles for both azimuth and elevation.

The composite PAS in azimuth of all clusters is modelled as wrapped Gaussian. The AOAs are determined by applying the inverse Gaussian function (7.5-9) with input parameters P_n and RMS angle spread ASA

$$\phi_{n,AOA}' = \frac{2(\mathrm{ASA}/1.4)\sqrt{-\ln(P_n/\max(P_n))}}{C_\phi},$$ (7.5-9)

with C_ϕ defined as

$$C_\phi = \begin{cases} C_\phi^{\mathrm{NLOS}} \cdot \left(1.1035 - 0.028K - 0.002K^2 + 0.0001K^3\right) & ,\text{for LOS} \\ C_\phi^{\mathrm{NLOS}} & ,\text{for NLOS} \end{cases},$$ (7.5-10)

where C_ϕ^{NLOS} is defined as a scaling factor related to the total number of clusters and is given in Table 7.5-2:

Table 7.5-2: Scaling factors for AOA, AOD generation

# clusters	4	5	8	10	11	12	14	15	16	19	20	25
C_ϕ^{NLOS}	0.779	0.860	1.018	1.090	1.123	1.146	1.190	1.211	1.226	1.273	1.289	1.358

In the LOS case, constant C_ϕ also depends on the Ricean K-factor K in [dB], as generated in Step 4. Additional scaling of the angles is required to compensate for the effect of LOS peak addition to the angle spread.

Assign positive or negative sign to the angles by multiplying with a random variable X_n with uniform distribution to the discrete set of $\{1,-1\}$, and add component $Y_n \sim N\left(0,(\mathrm{ASA}/7)^2\right)$ to introduce random variation

$$\phi_{n,AOA} = X_n \phi'_{n,AOA} + Y_n + \phi_{LOS,AOA},\qquad(7.5\text{-}11)$$

where $\phi_{LOS,AOA}$ is the LOS direction defined in the network layout description, see Step1c.

In the LOS case, substitute (7.5-11) by (7.5-12) to enforce the first cluster to the LOS direction $\phi_{LOS,\ AOA}$

$$\phi_{n,AOA} = \left(X_n \phi'_{n,AOA} + Y_n\right) - \left(X_1 \phi'_{1,AOA} + Y_1 - \phi_{LOS,AOA}\right)\qquad(7.5\text{-}12)$$

Finally add offset angles α_m from Table 7.5-3 to the cluster angles

$$\phi_{n,m,AOA} = \phi_{n,AOA} + c_{ASA}\alpha_m,\qquad(7.5\text{-}13)$$

where c_{ASA} is the cluster-wise rms azimuth spread of arrival angles (cluster ASA) in Table 7.5-6.

Table 7.5-3: Ray offset angles within a cluster, given for rms angle spread normalized to 1

Ray number m	Basis vector of offset angles α_m
1,2	± 0.0447
3,4	± 0.1413
5,6	± 0.2492
7,8	± 0.3715
9,10	± 0.5129
11,12	± 0.6797
13,14	± 0.8844
15,16	± 1.1481
17,18	± 1.5195
19,20	± 2.1551

The generation of AOD ($\phi_{n,m,AOD}$) follows a procedure similar to AOA as described above.

The generation of ZOA assumes that the composite PAS in the zenith dimension of all clusters is Laplacian (see Table 7.5-6). The ZOAs are determined by applying the inverse Laplacian function (7.5-14) with input parameters P_n and RMS angle spread ZSA

$$\theta'_{n,ZOA} = -\frac{\mathrm{ZSA}\ln\left(P_n/\max(P_n)\right)}{C_\theta},\qquad(7.5\text{-}14)$$

with C_θ defined as

$$C_\theta = \begin{cases} C_\theta^{\text{NLOS}} \cdot \left(1.3086 + 0.0339K - 0.0077K^2 + 0.0002K^3\right) & \text{, for LOS} \\ C_\theta^{\text{NLOS}} & \text{, for NLOS} \end{cases}, \quad (7.5\text{-}15)$$

Where C_θ^{NLOS} is a scaling factor related to the total number of clusters and is given in Table 7.5-4:

Table 7.5-4: Scaling factors for ZOA, ZOD generation

# clusters	8	10	11	12	15	19	20	25
C_θ^{NLOS}	0.889	0.957	1.031	1.104	1.1088	1.184	1.178	1.282

In the LOS case, constant C_θ also depends on the Ricean K-factor K in [dB], as generated in Step 4. Additional scaling of the angles is required to compensate for the effect of LOS peak addition to the angle spread.

Assign positive or negative sign to the angles by multiplying with a random variable X_n with uniform distribution to the discrete set of {1,–1}, and add component $Y_n \sim N\left(0, (\text{ZSA}/7)^2\right)$ to introduce random variation

$$\theta_{n,ZOA} = X_n \theta'_{n,ZOA} + Y_n + \overline{\theta}_{ZOA}, \quad (7.5\text{-}16)$$

where $\overline{\theta}_{ZOA} = 90°$ if the BS-UT link is O2I and $\overline{\theta}_{ZOA} = \theta_{LOS,ZOA}$ otherwise. The LOS direction is defined in the network layout description, see Step1c.

In the LOS case, substitute (7.5-16) by (7.5-17) to enforce the first cluster to the LOS direction $\theta_{LOS,ZOA}$

$$\theta_{n,ZOA} = \left(X_n \theta'_{n,ZOA} + Y_n\right) - \left(X_1 \theta'_{1,ZOA} + Y_1 - \theta_{LOS,ZOA}\right). \quad (7.5\text{-}17)$$

Finally add offset angles α_m from Table 7.5-3 to the cluster angles

$$\theta_{n,m,ZOA} = \theta_{n,ZOA} + c_{ZSA}\alpha_m, \quad (7.5\text{-}18)$$

where c_{ZSA} is the cluster-wise rms spread of ZOA (cluster ZSA) in Table 7.5-6. Assuming that $\theta_{n,m,ZOA}$ is wrapped within [0, 360°], if $\theta_{n,m,ZOA} \in [180°, 360°]$, then $\theta_{n,m,ZOA}$ is set to $(360° - \theta_{n,m,ZOA})$.

The generation of ZOD follows the same procedure as ZOA described above except equation (7.5-16) is replaced by

$$\theta_{n,ZOD} = X_n \theta'_{n,ZOD} + Y_n + \theta_{LOS,ZOD} + \mu_{offset,ZOD}, \quad (7.5\text{-}19)$$

where variable X_n is with uniform distribution to the discrete set of {1,–1}, $Y_n \sim N\left(0, (\text{ZSD}/7)^2\right)$, $\mu_{offset,ZOD}$ is given in Tables 7.5-6/7/8 and equation (7.5-18) is replaced by

$$\theta_{n,m,ZOD} = \theta_{n,ZOD} + (3/8)(10^{\mu_{\text{lgZSD}}})\alpha_m \quad (7.5\text{-}20)$$

where μ_{lgZSD} is the mean of the ZSD log-normal distribution.

In the LOS case, the generation of ZOD follows the same procedure as ZOA described above using equation (7.5-17).

<u>Step 8</u>: Coupling of rays within a cluster for both azimuth and elevation

Couple randomly AOD angles $\phi_{n,m,AOD}$ to AOA angles $\phi_{n,m,AOA}$ within a cluster n, or within a sub-cluster in the case of two strongest clusters (see Step 11 and Table 7.5-3). Couple randomly ZOD angles $\theta_{n,m,ZOD}$ with ZOA angles

$\theta_{n,m,ZOA}$ using the same procedure. Couple randomly AOD angles $\phi_{n,m,AOD}$ with ZOD angles $\theta_{n,m,ZOD}$ within a cluster n or within a sub-cluster in the case of two strongest clusters.

Step 9: Generate the cross polarization power ratios

Generate the cross polarization power ratios (XPR) κ for each ray m of each cluster n. XPR is log-Normal distributed. Draw XPR values as

$$\kappa_{n,m} = 10^{X_{n,m}/10},\tag{7.5-21}$$

where $X_{n,m} \sim N(\mu_{XPR}, \sigma_{XPR}^2)$ is Gaussian distributed with σ_{XPR} and μ_{XPR} from Table 7.5-6.

Note: $X_{n,m}$ is independently drawn for each ray and each cluster.

The outcome of Steps 1-9 shall be identical for all the links from co-sited sectors to a UT.

Coefficient generation:

Step 10: Draw initial random phases

Draw random initial phase $\left\{\Phi_{n,m}^{\theta\theta}, \Phi_{n,m}^{\theta\phi}, \Phi_{n,m}^{\phi\theta}, \Phi_{n,m}^{\phi\phi}\right\}$ for each ray m of each cluster n and for four different polarisation combinations ($\theta\theta, \theta\phi, \phi\theta, \phi\phi$). The distribution for initial phases is uniform within ($-\pi, \pi$).

Step 11: Generate channel coefficients for each cluster n and each receiver and transmitter element pair u, s.

The method described below is used at least for *drop-based evaluations* irrespective of UT speeds. Relevant cases for drop-based evaluations are:

- Case 1: For low complexity evaluations

- Case 2: To compare with earlier simulation results,

- Case 3: When none of the additional modelling components are turned on.

- Case 4: When spatial consistency and/or blockage is modeled for MU-MIMO simulations

- Other cases are not precluded

For the N – 2 weakest clusters, say $n = 3, 4,\ldots, N$, the channel coefficients are given by:

$$
\begin{aligned}
H_{u,s,n}^{\mathrm{NLOS}}(t) = \sqrt{\frac{P_n}{M}} \sum_{m=1}^{M} & \begin{bmatrix} F_{rx,u,\theta}\left(\theta_{n,m,ZOA}, \phi_{n,m,AOA}\right) \\ F_{rx,u,\phi}\left(\theta_{n,m,ZOA}, \phi_{n,m,AOA}\right) \end{bmatrix}^T \begin{bmatrix} \exp\left(j\Phi_{n,m}^{\theta\theta}\right) & \sqrt{\kappa_{n,m}^{-1}}\exp\left(j\Phi_{n,m}^{\theta\phi}\right) \\ \sqrt{\kappa_{n,m}^{-1}}\exp\left(j\Phi_{n,m}^{\phi\theta}\right) & \exp\left(j\Phi_{n,m}^{\phi\phi}\right) \end{bmatrix} \\
& \begin{bmatrix} F_{tx,s,\theta}\left(\theta_{n,m,ZOD}, \phi_{n,m,AOD}\right) \\ F_{tx,s,\phi}\left(\theta_{n,m,ZOD}, \phi_{n,m,AOD}\right) \end{bmatrix} \exp\left(\frac{j2\pi\left(\hat{r}_{rx,n,m}^T.\overline{d}_{rx,u}\right)}{\lambda_0}\right) \exp\left(\frac{j2\pi\left(\hat{r}_{tx,n,m}^T.\overline{d}_{tx,s}\right)}{\lambda_0}\right) \exp\left(j2\pi\frac{\hat{r}_{rx,n,m}^T.\overline{v}}{\lambda_0}t\right)
\end{aligned}\tag{7.5-22}
$$

where $F_{rx,u,\theta}$ and $F_{rx,u,\phi}$ are the field patterns of receive antenna element u according to (7.1-11) and in the direction of the spherical basis vectors, $\hat{\theta}$ and $\hat{\phi}$ respectively, $F_{tx,s,\theta}$ and $F_{tx,s,\phi}$ are the field patterns of transmit antenna element s in the direction of the spherical basis vectors, $\hat{\theta}$ and $\hat{\phi}$ respectively. Note that the patterns are given in the GCS and therefore include transformations with respect to antenna orientation as described in Clause 7.1. $\hat{r}_{rx,n,m}$ is the spherical unit vector with azimuth arrival angle $\phi_{n,m,AOA}$ and elevation arrival angle $\theta_{n,m,ZOA}$, given by

$$\hat{r}_{rx,n,m} = \begin{bmatrix} \sin\theta_{n,m,ZOA}\cos\phi_{n,m,AOA} \\ \sin\theta_{n,m,ZOA}\sin\phi_{n,m,AOA} \\ \cos\theta_{n,m,ZOA} \end{bmatrix},$$

(7.5-23)

where n denotes a cluster and m denotes a ray within cluster n. $\hat{r}_{tx,n,m}$ is the spherical unit vector with azimuth departure angle $\phi_{n,m,AOD}$ and elevation departure angle $\theta_{n,m,ZOD}$, given by

$$\hat{r}_{tx,n,m} = \begin{bmatrix} \sin\theta_{n,m,ZOD}\cos\phi_{n,m,AOD} \\ \sin\theta_{n,m,ZOD}\sin\phi_{n,m,AOD} \\ \cos\theta_{n,m,ZOD} \end{bmatrix},$$

(7.5-24)

where n denotes a cluster and m denotes a ray within cluster n. Also, $\bar{d}_{rx,u}$ is the location vector of receive antenna element u and $\bar{d}_{tx,s}$ is the location vector of transmit antenna element s, $\kappa_{n,m}$ is the cross polarisation power ratio in linear scale, and λ_0 is the wavelength of the carrier frequency. If polarisation is not considered, the 2x2 polarisation matrix can be replaced by the scalar $\exp(j\Phi_{n,m})$ and only vertically polarised field patterns are applied.

The Doppler frequency component depends on the arrival angles (AOA, ZOA), and the UT velocity vector $\bar{v}$ with speed v, travel azimuth angle ϕ_v, elevation angle θ_v and is given by

$$v_{n,m} = \frac{\hat{r}_{rx,n,m}^T \cdot \bar{v}}{\lambda_0}, \text{ where } \bar{v} = v.[\sin\theta_v\cos\phi_v \quad \sin\theta_v\sin\phi_v \quad \cos\theta_v]^T.$$

(7.5-25)

For the two strongest clusters, say $n = 1$ and 2, rays are spread in delay to three sub-clusters (per cluster), with fixed delay offset. The delays of the sub-clusters are

$$\begin{aligned} \tau_{n,1} &= \tau_n \\ \tau_{n,2} &= \tau_n + 1.28\ c_{DS} \\ \tau_{n,3} &= \tau_n + 2.56\ c_{DS} \end{aligned}$$

(7.5-26)

where c_{DS} is cluster delay spread specified in Table 7.5-6. When intra-cluster delay spread is unspecified (i.e., N/A) the value 3.91 ns is used; it is noted that this value results in the legacy behaviour with 5 and 10 ns sub-cluster delays.

Twenty rays of a cluster are mapped to sub-clusters as presented in Table 7.5-5 below. The corresponding offset angles are taken from Table 7.5-3 with mapping of Table 7.5-5.

Table 7.5-5: Sub-cluster information for intra cluster delay spread clusters

sub-cluster # i	mapping to rays R_i	Power $|R_i|/M$	delay offset $\tau_{n,i} - \tau_n$
$i = 1$	$R_1 = \{1,2,3,4,5,6,7,8,19,20\}$	10/20	0
$i = 2$	$R_2 = \{9,10,11,12,17,18\}$	6/20	1.28 c_{DS}
$i = 3$	$R_3 = \{13,14,15,16\}$	4/20	2.56 c_{DS}

Then, the channel impulse response is given by:

$$H_{u,s}^{\text{NLOS}}(\tau,t) = \sum_{n=1}^{2}\sum_{i=1}^{3}\sum_{m\in R_i} H_{u,s,n,m}^{\text{NLOS}}(t)\delta(\tau - \tau_{n,i}) + \sum_{n=3}^{N} H_{u,s,n}^{\text{NLOS}}(t)\delta(\tau - \tau_n)$$

(7.5-27)

where $H_{u,s,n}^{\text{NLOS}}(t)$ is given in (7.5-22) and $H_{u,s,n,m}^{\text{NLOS}}(t)$ defined as:

$$
H_{u,s,n,m}^{\text{NLOS}}(t) = \sqrt{\frac{P_n}{M}} \begin{bmatrix} F_{rx,u,\theta}(\theta_{n,m,ZOA}, \phi_{n,m,AOA}) \\ F_{rx,u,\phi}(\theta_{n,m,ZOA}, \phi_{n,m,AOA}) \end{bmatrix}^T \begin{bmatrix} \exp(j\Phi_{n,m}^{\theta\theta}) & \sqrt{\kappa_{n,m}^{-1}}\exp(j\Phi_{n,m}^{\theta\phi}) \\ \sqrt{\kappa_{n,m}^{-1}}\exp(j\Phi_{n,m}^{\phi\theta}) & \exp(j\Phi_{n,m}^{\phi\phi}) \end{bmatrix}
$$

$$
\begin{bmatrix} F_{tx,s,\theta}(\theta_{n,m,ZOD}, \phi_{n,m,AOD}) \\ F_{tx,s,\phi}(\theta_{n,m,ZOD}, \phi_{n,m,AOD}) \end{bmatrix} \exp\left(j2\pi\frac{\hat{r}_{rx,n,m}^T.\bar{d}_{rx,u}}{\lambda_0}\right)\exp\left(j2\pi\frac{\hat{r}_{tx,n,m}^T.\bar{d}_{tx,s}}{\lambda_0}\right)\exp\left(j2\pi\frac{\hat{r}_{rx,n,m}^T.\bar{v}}{\lambda_0}t\right) \tag{7.5-28}
$$

In the LOS case, determine the LOS channel coefficient by:

$$
H_{u,s,1}^{\text{LOS}}(t) = \begin{bmatrix} F_{rx,u,\theta}(\theta_{LOS,ZOA}, \phi_{LOS,AOA}) \\ F_{rx,u,\phi}(\theta_{LOS,ZOA}, \phi_{LOS,AOA}) \end{bmatrix}^T \begin{bmatrix} 1 & 0 \\ 0 & -1 \end{bmatrix} \begin{bmatrix} F_{tx,s,\theta}(\theta_{LOS,ZOD}, \phi_{LOS,AOD}) \\ F_{tx,s,\phi}(\theta_{LOS,ZOD}, \phi_{LOS,AOD}) \end{bmatrix}
$$

$$
\cdot \exp\left(-j2\pi\frac{d_{3D}}{\lambda_0}\right)\exp\left(j2\pi\frac{\hat{r}_{rx,LOS}^T.\bar{d}_{rx,u}}{\lambda_0}\right)\exp\left(j2\pi\frac{\hat{r}_{tx,LOS}^T.\bar{d}_{tx,s}}{\lambda_0}\right)\exp\left(j2\pi\frac{\hat{r}_{rx,LOS}^T.\bar{v}}{\lambda_0}t\right) \tag{7.5-29}
$$

where $\delta(\cdot)$ is the Dirac's delta function and K_R is the Ricean K-factor as generated in Step 4 converted to linear scale.

Then, the channel impulse response is given by adding the LOS channel coefficient to the NLOS channel impulse response and scaling both terms according to the desired K-factor K_R as

$$
H_{u,s}^{\text{LOS}}(\tau,t) = \sqrt{\frac{1}{K_R+1}}H_{u,s}^{\text{NLOS}}(\tau,t) + \sqrt{\frac{K_R}{K_R+1}}H_{u,s,1}^{\text{LOS}}(t)\delta(\tau-\tau_1). \tag{7.5-30}
$$

Step 12: Apply pathloss and shadowing for the channel coefficients.